We thank reviewer 1 for his valuable comments and suggestions and we will consider these comments in the revised version. In the following we address each of the major and minor comments given by reviewer 1. Pages and lines indicating modifications refer to the revised manuscript version, including track changes.

1. Abstract: the term 'dislocated' is not appropriate. Suggest 'dislodged' instead.

Ok, we changed to dislodged (p. 1, line 19).

2. Abstract: change 'uphill' to 'upslope'.

Ok, we changed to upslope (p. 1, line 22)

3. Abstract: the authors state that the high flow velocity calculations from boulder measurements exceed flows predicted by a hydrodynamic model, and that this therefore supports the notion of infragravity waves produced by Typhoon Haiyan. But it may also point towards the underperformance of the hydrodynamic model. Please address briefly.

Indeed, the discrepancy also results from the underperformance of the hydrodynamic model: a possible explanation would be a limited spatial resolution (e.g., of the local bathymetry and topography) of the model input data. However, Bricker and Roeber (2015) recently presented such a detailed Delft3D-based model for Hernani using own bathymetric mapping in the sheltered bay off of the town; generally infer very similar conclusions. The main reason for the discrepancy between the flow velocities calculated from boulder measurements and the application of initiation-of-motion criteria, and those predicted by the hydrodynamic model, is thus due to the fact that phase-averaged models such as Delft3D cannot resolve the influence of infragravity waves. While we cannot incorporate this discussion into the abstract (see section 6.2 for further discussion), we have added a note on the recently published phase-resolving wave models (e.g. Shimozono et al., 2015). It should now be clear for the reader that the discrepancies also imply underperformances of the presented model (p. 1, lines 26ff)

4. Abstract: 'demand to carefully reassess' - please rephrase.

Ok, we rephrased the sentence to "…demand a careful re-evaluation of storm-related transport…. " (p. 2, lines 2-3)

5. Course of the event: correct to 'in a westward direction...'

We changed the sentence accordingly (p. 3, line 27).

6. Coastal flooding: correct to 'similar to how TC Nargis...'

We changed the sentence accordingly (p. 4, line 13).

7. Previous typhoons: use 'Eastern Samar' throughout instead of 'E Samar'. Currently both are used.

Ok, we changed to Eastern Samar.

8. Field and laboratory work: multi-view image methods for coastal boulder size estimation were recently published by Gienko (2014), ESPL, v.39, p.853–864.

Thanks, we included the reference (p. 7, line 5).

9. Field evidence: change 'subrecent transport' to 'historical transport'

We changed to “recent transport”; “historical transport” refers to the 13 further clasts that “must have been transported by a previous event based on their mature vegetation cover” (p. 9, line 6).

10. Storm surge and wave model: please rephrase 'the here presented Delft3D model'.

Ok, we rephrased this section (p. 11, line 20)

11. Boulder transport and flow velocities: the authors admit that 'flow velocities modeled with Delft3D are insufficient to account for the transport of the documented clasts'. This leads on to their proposal that this is evidence for a range of hydrodynamic processes having been responsible for the movement of the large coastal clasts. Although I do not necessarily disagree with this, I feel this issue could benefit from further consideration. The discrepancy in flow results may have several alternative explanations, either that the flows calculated using the transport equations are overestimated, or that the flows determined by the model are underestimated, or likely both to some unknown degree. The authors could make a valuable contribution here, providing more discussion on how to proceed in such cases where multiple methodologies used for the best intentions (i.e. validation) then yield results that are not in agreement.

We agree that the applied formulae are simplifying and depend on a number of coefficients (i.e., coefficients of lift, drag, or static friction). However, it has been shown that they can produce reasonable estimates of minimum flow velocities needed for the transport of large clasts. The use of case-sensitive coefficients and/or the application of min/max values for these coefficients given by previous studies (Nott, 2003; Noormets et al., 2004; Benner et al., 2010; Paris et al., 2010; Nandasena et al., 2011) results in even higher velocities in most cases. Thus, when following previous studies (e.g., Paris et al., 2010; Nandasena et al., 2011) and applying these equations, it seems that overestimation by the applied equations can be excluded – the flow velocities presented here are therefore interpreted to represent minimum values for the transport of the clasts. We will briefly discuss the influence of the use of case-sensitive coefficients (drag, lift, and friction) in the revised version of the manuscript.

As to the underestimation of flow velocities by the presented hydrodynamic model, we agree that higher resolution models may indeed result in more realistic estimation of flow velocities for the study area. Bricker and Roeber (2015) recently presented such a detailed model for Hernani based on own bathymetric mapping in the sheltered bay off of the town. Nevertheless, they generally infer very similar conclusions. Thus, the discrepancy (as stated before) results from the underperformance of phase-averaged models such as Delft3D, which cannot resolve the influence of infragravity waves. We also mention the study of Bricker and Roeber (2015) in lines 28ff on page 11.

Modifications: 5.3, page 10, lines 13ff; 6.1, page 13, lines 23ff

12. Conclusions: 'a variety of hydrodynamic processes .... must be considered when interpreting boulder deposits...' This is too a vague statement to include in the conclusions, especially since this is one of the main thrusts of this paper. Please be more specific. List and briefly outline these various processes.

We have changed the conclusions in the revised version accordingly, now specifically listing and outlining the various processes potentially being involved in the boulder movement (p. 17, lines 3ff).

We thank reviewer 2 for the critical comments and suggestions. We will consider these comments in the revised version. Each of the major and minor comments given by reviewer 2 will be addressed in the following. Pages and lines indicating modifications refer to the revised manuscript version, including track changes.

1. P.747, L10: How did the authors determine the coefficients of drag, lift forces and static friction for each boulder? The coefficients should be different especially between round-shaped and slab-shaped boulders. The static friction should also be different on the beach and terrace behind it. Please discuss uncertainty associated with the choice of these coefficients.

We agree with reviewer 2. Since we cannot present empirical data on e.g. the coefficient of static friction or lift, we – as most previous studies – generally rely on the use of coefficients taken from literature. However, some authors give certain ranges (with min and max values) for these coefficients, the use of which apparently results in different minimum flow velocities required for the transport of the clasts:

Several authors have used 0.7 for the coefficient of static friction, e.g. on basalt or on sand-covered limestone platforms (Noormets et al., 2004; Paris et al., 2010; Nandasena et al., 2011); Goto et al. (2007) applied 0.75 for a sand-covered limestone platform, and Buckley et al. (2012) used 0.6 +- 0.2 in their study. Likewise, Benner et al. (2010), give values of 0.6 or 0.65-0.8 as possible values for static friction, which only slightly differ from 0.7. However, Nott (2003) refers to the empirical study of Fukui et al. (1963) and introduced friction factors between 0.82-1.02. When applying min and max values given in Nott (2003), the results (i.e., flow velocities required for the transport of the clasts) change by the order of 0.2 m/s.

For the coefficient of lift we used 0.178, similar to several previous studies (Nott, 2003; Noormets et al., 2004; Paris et al., 2010; Nandasena et al., 2011). However, Benner et al. (2010) state that every value between 0.05 and 0.2 may be realistic, with the maximum value being close to the one used in our study and in the previous studies. When applying the minimum value given in Benner et al. (2010) (0.05), then flow velocities would increase by 0.5-0.7 m/s for rolling/sliding, and up to ~20 m/s for saltation/lifting. We thus think that, for the estimation of minimum flow velocities, the values for coefficient of lift used in our study are conservative values.

However, as to the coefficient of drag (Cd), we introduced boulder-specific values in the revised version: Noormets et al. (2004) refer to Fig. 3 in Helley (1969) illustrating the relationship of the shape of a clast transported by flowing water (i.e., expressed by the Corey shape factor; Corey, 1949) and the Cd it experiences. Accordingly, different shape factors are calculated for ESA 7 and ESA 9 (0.73 and 0.55), and thus different Cd values may be inferred when following Noormets et al. (2004). Applying these boulder-specific shape factors and taking the boulder-appropriate Cd factors from Helley (1969) (ESA 7: 0.85-1.15, ESA 9: 1.4-1.8), minimum flow velocities necessary for the transport of ESA 7 increase by 1.5-2.5 m/s, for ESA 9 to 0.3 and 1.2 m/s.

We will incorporate the most important aspects of this discussion in the revised text to clarify the choice of the various coefficients. Since boulder-specific values for Cd can be inferred, we will include these new values in the revised version.

Modifications: 6.1, page 13, lines 23ff

2. P.750 L2: b and c in equations (1)-(3) are defined as the second longest axis and the shortest axis. I think they are not appropriate definitions as the force balance would become *independent of the boulder direction to the flow. The choice of b and c may significantly affect the minimum velocity especially for the elongated boulder such as ESA9. On the other hand, a, b, c are defined as length, width and height in 4.2. The definitions should be consistent throughout the paper.*

We agree that the definitions of a, b and c axes should be consistent throughout the paper, and that the denominations "longest, second longest and shortest axis" may be misleading since it is disregarding the position of the boulder to the flow. We have thus changed the definitions given in line 2, page 12, to "width" and "height". However, in all cases, the longest axis of the investigated clast referred to length (a-axis), the second longest axis was the width of the boulder (b-axis), and the shortest axis was the height of the boulder (c-axis). The values used for the boulder axes in the Nandasena equations are thus in the correct relation to force balance.

Modifications: page 10, lines 14ff

3. P.750, L16: Is it appropriate to apply Nandasena's equations for ESA5? It was originally located at the cliff edge where flow velocity could have a vertical component locally, or wave splash-up could exert impact force on it.

The calculation of flow velocities for joint-bounded ESA 5 using Nandasena's equations are indeed related to uncertainties. We have mentioned that JBB scenarios tend to produce overestimated values, and that "discrepancies may for instance be related to the overestimation of strain forces between the block and the strongly karstified reef body, or to the underestimation of the waves' impact and lift forces approaching the cliffs and their associated jets (Hansom et al., 2008)". On the other hand, one may also assume that ESA 5 was already submerged during the initiation of motion due to storm surge and wave setup and resulting elevated water levels, and vertical jets/wave splash-up may have thus had a reduced influence; little is known about flow velocity amplification along cliffs under submerged conditions.

However, for this reason, the value derived for ESA 5 by the JBB scenario is not used in the following discussion; we have used the minimum velocities calculated for ESA 7 and 9 for comparison with the survivor video and the recently published models of infragravity waves.

Modifications: we extended the discussion in section 6.1; however, we think that we have clearly stated uncertainties related to the JBB scenario in the text (page 14, lines 16ff).

4. P. 751, L3: The maximum significant wave height of 4-6 m off the coast is too small for one induced by the super typhoon with extreme winds. Many others commonly estimated the value between 15 and 20 m. Roeber and Bricker estimated it as 19.7 m off Hernani. This discrepancy is beyond the range of uncertainty of wave hindcast model.

We agree that the discrepancy is beyond the range of uncertainty if we compare it with lowest resolution models presented in previous studies (Bricker et al., 2014), or with the details given in Roeber and Bricker (2015). Interestingly, the higher resolution Delft3D-based models provided in these studies nevertheless seem to show wave heights comparable to our study.

Most likely, the discrepancy in wave height is caused by the different tracks used in our simulation (JTWC storm track) compared to previous studies (JMA storm track). In the JMA storm track, used in e.g. Bricker et al. (2014), where >15 m significant wave heights were produced in the 2.5 km model, 10-min sustained winds are implemented, which is in contrast to the 1-min sustained winds implemented in the JTWC track used in our model. Generally, 10-min sustained winds are lower compared to 1-min sustained winds, but higher wind velocities (V) correspond to smaller wind radii (R). We compared the R_{max} used in our study to those used in the Bricker study obtained from Quiring's relation.

	R_{max} (NM)		V_{max} (KTS)	
TIME (UTC)	JMA (Bricker)	JTWC (May)	JMA (Bricker)	JTWC (May)
201311071200	19.47	17	125	170
201311071800	19.47	17	125	170
201311080000	23.09	15	110	165
201311080600	27.93	10	90	145

This could explain the lower wave heights resulting from our model. Since we have higher values for V_{max} (i.e. lower values for R_{max}), the area affected/reached by the maximum sustained wind is smaller. Most probably, maximum sustained winds in our model thus affected a smaller area compared to those implemented in the JMA track with 10-min sustained winds.

However, a simple reproduction of previous models cannot be the purpose of our study. We thus decided to keep our model in the paper, but to point out the underestimations and discrepancies and their possible reasons, and to refer to the previously published models for transparency.

Despite the mentioned discrepancies, the conclusions inferred from the previously published models are similar to the ones presented here – flow velocities (as a result of pressure and wind driven storm surge and wave setup) remain clearly below those required to transport the clasts at ESA. We thus feel certain that the main conclusions of our paper will remain the same, even though the presented model does not reproduce previous ones.

Modifications: page 13, lines 1ff (while we keep the description of the model output in the results sections similar to the one in the previous version of our paper, we have included a new section referring to the underestimations and possible explanations of model discrepancies in the discussion section (6.1)).

5. Figure 8c: When was the maximum wave height resulted at ESA site? I suggest an additional figure of wave height distribution in the same area as Fig 8c at the timing of the highest wave development. There is no information provided on local wave characteristics and how much waves were underestimated by the phase-averaged model.

We thank reviewer 2 for this comment. Although the wave height is differing from the previously published models, the timing of maximum significant wave heights in our model is generally in agreement with the generation of the infragravity waves video captured at ~6 a.m. PHT (local time), and thus with the occurrence of max. wave heights at Hernani: Figure 8a shows max. significant wave heights at the timing of the highest wave development, which started – according to our model – at ~5.20 a.m. PHT (depicted in Fig. 8a) and lasted until ~6 a.m., while highest flow velocities (due to pressure- and wind-induced setup) occurred delayed (Fig. 8b,c). This is in agreement with the information given in Roeber and Bricker (2015), stating that modeled offshore wave heights dropped rapidly after 6.a.m., “even though the pressure- and wind-induced setup persisted. Since the pressure and wind-driven setup lagged the offshore sea state, only a short time window existed for the surf beat to reach its most destructive form" (Roeber and Bricker, 2015: 8).

However, due to the comparably low resolution of our model, in our opinion it is not constructive to present a further subfigure showing wave height distribution in the same area as Fig 8c at the timing of the highest wave development; no additional information would be provided. We have added a note/further explanation on the timing of max. wave heights (see above). We will also add some information on local wave characteristics to the revised manuscript.

Modifications: page 13, lines 1ff; page 15, lines 31ff; page 4, lines 8f.

6. Figure 8c: The velocity field developed along the coastline looks mostly due to storm surges and there seems to be very small contribution from the wave-induced velocity. The authors emphasize the agreement of the flow direction and boulder trajectories implying that the boulder transport is attributed to the flow (P.752, 13). This sounds a bit contradictory to the later discussion on the importance of infragravity bore-like waves which is lacking in the model. Please explain more on this.

We agree with reviewer 2 that our text implies a relation between the flow direction illustrated by the Delft3D model and the boulder trajectories, and we agree that this sounds contradictory since the high flow velocities must be explained by the occurrence of infragravity waves. However, we have to point out that there is a coincidence of the modeled flow vectors with the transport direction of the boulders, which we cannot fully explain. We have thus tried to clarify this point in the revised version by mentioning this particular transport direction and a possible deflection of infragravity wave-driven reef-top currents (see next comment).

Modification: page 12, lines 25f, and page 16, lines 6ff.

7. 6.2: I agree with the authors that the extreme flows on the coast cannot be explained without the presence of infragravity waves, which were also illustrated by Roeber and Bricker (2015) and Shimozono et al (2015). A question arises as to whether the borelike waves similar to one observed in Hernani can be generated in shore-parallel direction because the large-scale boulder transport occurs along the shore. It may be worth mentioning this point.

We agree, and we will mention/point out this specific point. Deflection along the cliff coast may potentially play a role in the direction of infragravity wave-driven water currents on top of the reef platform.

Modification: 6.2, page 16, lines 6ff.

References used (in addition to those cited in the original text)

Corey, A.T., 1949. Influence of shape on fall velocity of sand grains. Unpublished Msc thesis, Colorado A&M College, 102 pp.

Fukui, Y., Nakamura, M., Shiraishi, H., and Sasaki,Y ., 1963. Hydraulic study on tsunami: Coastal Engineering in Japan, 6, 67-82.

Helley, E.J., 1969. Field measurement of the initiation of large bed particle motion in blue creek near Klamath, California. U.S. Geological Survey Professional Paper 562-G (19 pp.).

Bricker, J. and Roeber, V.: Mechanisms of damage during Typhoon Haiyan: storm surge, waves, and "tsunami-like" surf beat, E-proceedings of the 36th IAHR World Congress, 28 June–3 July, 2015, The Hague, the Netherlands, 2015.

Benner, R., Browne, T., Brückner, H., Kelletat, D., and Scheffers, A., 2010. Boulder Transport by Waves: Progress in Physical Modelling. Zeitschrift für Geomorphologie, 54, Suppl. 3, 127-146.

Block and boulder transport in Eastern Samar (Philippines) during Supertyphoon Haiyan

S.M. May[1], M. Engel[1], D. Brill[1], C. Cuadra[2], A.M.F. Lagmay[2,3], J. Santiago[2], J.K. Suarez[2], M. Reyes[4], H. Brückner[1]

[1]{Institute of Geography, Universität zu Köln, Albertus-Magnus-Platz, 50923 Köln (Cologne), Germany}

[2]{Project NOAH (Nationwide Operational Assessment of Hazards), Department of Science and Technology, Quezon City, Philippines}

[3]{National Institute of Geological Sciences, University of the Philippines Diliman, Philippines / Project NOAH (Nationwide Operational Assessment of Hazards), Department of Science and Technology, Quezon City, Philippines}

[4]{Marine Science Institute, University of the Philippines, Velasquez St., Diliman, Quezon City 1101, Philippines}

Correspondence to: S.M. May (mays@uni-koeln.de)

Abstract

Fields of dislodged ~~dislocated~~ boulders and blocks record catastrophic coastal flooding during strong storms or tsunamis and play a pivotal role in coastal hazard assessment. Along the rocky carbonate coast of Eastern Samar (Philippines) we documented longshore transport of a block of 180 t and boulders (up to 23.5 t) shifted ~~uphill~~ upslope to elevations of up to 10 m above mean lower low water level during Supertyphoon Haiyan on 8 Nov 2013. Initiation-of-motion approaches indicate that boulder dislocation occurred with flow velocities of 8~~6~~.9~~3~~–9~~8~~.6~~3~~ m s-1 which significantly exceeds depth-averaged flow velocities of a local coupled hydrodynamic and wave model (Delft3D) of the typhoon with a maximum <1.5 m s-1. These results, in combination with recently ~~presented~~published phase-resolving ~~support~~wave models, support the hypothesis that infragravity waves induced by the typhoon were responsible for the remarkable flooding pattern in ~~E Samar~~Eastern Samar, which are not

Formatiert: Nicht Hervorheben

Formatiert: Nicht Hervorheben

Formatiert: Nicht Hervorheben

resolved in phase-averaged storm surge models. Our findings show that tsunamis and hydrodynamic conditions induced by tropical cyclones may shift boulders of similar size and, therefore, demand ~~to~~ a careful~~ly~~ ~~reassess~~ re-evaluation of ~~the possibility of~~ storm-related transport where it, based on the boulder's sheer size, has previously been ascribed to tsunamis.

Formatiert: Nicht Hervorheben

1 Introduction

Fields of dislocated boulders and blocks are among the most impressive sedimentary evidence of catastrophic coastal flooding (Williams and Hall, 2004; Scicchitano et al., 2007; Etienne et al., 2011; Goto et al., 2010, 2011; Nandasena et al., 2011; Richmond et al., 2011; Engel and May, 2012; Terry et al., 2013) and are widely used to infer the most extreme magnitudes of marine flooding events (tsunamis, storm surges) over large time scales (Etienne et al., 2011; Engel and May, 2012; Terry et al., 2013). Criteria to distinguish between tsunamis and storms include exponential landward fining of boulder fields or the generation of ridges due to strong storms, and more random scattering of boulders through tsunamis (Goto et al., 2010; Richmond et al., 2011). For some boulder deposits, storm transport was ruled out based on their large size, elevation and distance from the coast, and local extreme storm wave conditions (Scicchitano et al., 2007; Engel and May, 2012), while the long wave period of tsunamis has been associated with a higher transport competence (Lorang, 2011). However, the topic is still vividly debated (Goto et al., 2010; Lorang, 2011); until recently, only few studies provided unambiguous evidence for the transport of very large clasts during storms (Goto et al., 2011), e.g. based on direct observations, reliable historical documentation, or satellite data (Table 1). However, dimensions and transport distances of these clasts are often significantly smaller than those of palaeo-deposits for which the mode of transport is unknown.

We present evidence for onshore block and boulder dislocation at the carbonate coast of Eastern Samar (Philippines; Fig. 1) during Supertyphoon Haiyan (local name: Yolanda), one of the strongest tropical cyclones (TC) on record. Using sedimentary parameters of the clasts (spatial distribution, size, orientation, etc.), bi-temporal satellite images, characteristics of the storm surge and waves inferred from local numerical models, and inverse modelling of minimum flow velocities required to initiate boulder movement, we provide insights into the hydrodynamic and sedimentary processes during a TC. These insights have important implications for the boulder-related "storm vs. tsunami" debate.

2 Physical setting

Situated directly north of Leyte, the island of Samar is part of the Eastern Visayas (Philippines) (Fig. 1a). It is facing the Philippine Sea with the Philippine Trench and subduction zone to the east and the Philippine Fault to the west, the latter comprising a 1200 km long system of strike-slip faults crossing Leyte in a NW-SE direction (Barrier et al., 1991; Ramos and Tsutsumi, 2010). The inner part of Samar consists of Cretaceous to Oligocene igneous rocks, surrounded by mostly carbonate rocks of Mio-Pliocene age showing typical karst morphology (Traveglia et al., 1978).

Along the coast of ~~E Samar~~Eastern Samar, Holocene fringing coral reefs are up to several hundred meters wide (Fig. 1b). Offshore, the bathymetry immediately drops down towards the Philippine Trench. Similar to other coastal areas in the Philippines, elevated reef terraces of last interglacial age (e.g., Omura et al., 2004) are present along the ~~E Samar~~Eastern Samar coast as well, e.g. near the municipality of Hernani, where this study was conducted. Based on our DGPS measurements, the tidal range at site ESA on 17 Feb 2014 amounted to 1.5 m, which is similar to the tidal range of Laong (N Samar) given in Maeda et al. (2004).

3 Supertyphoon Haiyan

3.1 Course of the event

Originating from a tropical depression which formed on November 3rd 2013 over the northwestern Pacific, Supertyphoon Haiyan turned into a tropical storm on November 4th and gained typhoon status on November 5th. On November 6th Haiyan reached the status of a category 5 cyclone on the Saffir-Simpson Hurricane scale and made landfall near Guiuan (Eastern Samar) at 4:40 am on November 8th (IRIDeS, 2014; Lagmay et al., 2015). Haiyan crossed the entire archipelago in a westward direction ~~in western direction~~ without falling below category 5 on the Saffir-Simpson hurricane scale (Figs 1a, 2). Further landfalls occurred at 7:00 am on northern Leyte (close to Dulag), and later on northern Cebu, Panay and Palawan. Due to sustained wind speeds of 314 km h^{-1} (1-minute average based on remote

Formatiert: Englisch (USA)

sensing data) and a heavy storm surge leading to rapid, extensive flooding, Haiyan was an extraordinary natural disaster causing 6,268 casualties and affecting more than 16 M people (Lagmay et al., 2015).

3.2 Coastal flooding and hazard response

Coastal flooding rapidly reached peak levels that lasted for approximately two hours. It was locally characterized by multiple pulses of inflowing waves with periods of several seconds (Mas et al., 2015); eyewitnesses on Leyte and Samar reported a threefold withdrawal of the sea followed by distinct flooding pulses~~.~~ , and waves superimposing the storm surge reached up to 4 m in Tacloban. In Eastern Samar, wave periods of 10-20 s were reported (Mas et al., 2015). High flow velocities of uprushing currents were inferred from a survivor video at Hernani, which approached for more than 1 minute before receding (Gensis, 2013; Bricker and Roeber, 2015; Mas et al., 2015). Post-typhoon interviews with residents suggest that, similar to ~~similar to~~ how TC Nargis ~~as TC Nargis~~ had impacted Myanmar's Ayeyarwady delta in 2008 (Fritz et al., 2009), the coastal population of Leyte and ~~E Samar~~Eastern Samar lacked a proper understanding of the dimensions and devastating effects potentially connected with the term "storm surge". This lack of awareness is typically linked to the low frequency of such highest-magnitude events (Fritz et al., 2009), a relationship best described by inverse power-law functions (Corral et al., 2010). Personal experience and adaptation is commonly restricted to events of much smaller magnitude. This classical relationship emphasizes the pivotal role of geological records of extreme-wave events for coastal hazard assessment as they may provide information on local to regional frequency-magnitude patterns over millennial timescales and can also be implemented in education and raising awareness among residents (Weiss and Bourgeois, 2012).

The exposed coast of Eastern Samar is characterized by a large fetch and a steep offshore bathymetry. Hence, it experienced maximum wind speeds with the highest model-predicted waves of up to 19 m, but only a limited wind-driven surge during Haiyan (Bricker et al. 2014). Field indicators document inundation levels of up to 6 m onshore flow depth, nearly 11 m run-ups above local event tide level, and inundation distances of up to 800 m depending on onshore topography (PAGASA, 2014; Tajima et al. 2014; Shimozono et al., 2015).

3.3 Previous Typhoons and storm systems

~~E Samar~~Eastern Samar has repeatedly been impacted by severe typhoons in the historical past although they are generally less frequent compared to coastal areas further north. Catastrophic typhoons with tracks similar to the one of Haiyan occurred on 12–13 Oct 1897 (Algué, 1898), on 24–25 Nov 1912 (Philippine Weather Bureau, 1912), and on 4 Nov 1984 (Typhoon Undang/Agnes, category 4 on SSHS) (JTWC, 1985). However, on historical time scales, Supertyphoon Haiyan is supposed to be the strongest typhoon to have hit ~~E Samar~~Eastern Samar (Lapidez et al., 2015).

Pre-Haiyan satellite images available for comparison with images captured after Haiyan date to 4 May 2013. Post-Haiyan images were captured three days after the typhoon on 11 November 2013, thereby excluding subsequent typhoons such as Basyang (31 Jan 2014; NDRRMC, 2014) for coarse-clast transport. Between 4 May 2013 and 08 November 2013, three storm systems occurred within an area of c. 250 km N, S, and E of ~~E Samar~~Eastern Samar, according to the typhoon database of the Joint Typhoon Warning Center (JTWC, 2014). The tracks of two of these storm systems crossed an area of 120 km surrounding the study area, extending from the northern tip of Mindanao to northern Samar (Fig. 2). Tropical storm 30W (3 Nov–06 Nov 2013) only reached moderate wind speeds of ≤60 km h^{-1} when passing the 120 km radius, and its atmospheric pressure remained above 1000 hPa. Typhoon Rumbia (27 Jun–02 Jul 2013) had a northern track and made landfall at the City of Taft some 65 km north of the study area. However, it had maximum wind speeds of ≤64 km h^{-1} and reached a minimum atmospheric pressure of 996 hPa while approaching the coasts of ~~E Samar~~Eastern Samar and Leyte. Based on the low number of storm systems between May and November 2013 and their rather moderate intensity compared to Supertyphoon Haiyan, we ascribe any major block and boulder transport inferred from the satellite images to the latter event.

4 Methods and data

4.1 Interpretation of satellite images

Panchromatic satellite images of World View 1 (WV1, ID 1020010021141100, 4 May 2013) and WV2 (ID 10300100294524000, 11 Nov 2013) were used for mapping of the pre- and post-Haiyan position of wave-transported large clasts between Hernani and the study site. The original georeferenced images were aligned based on unaltered coastal structures such as cliff edges using ESRI ArcGIS software, resulting in a positional accuracy of ~2 pixel (~1.2 m). Satellite image-based mapping was restricted to clasts which were not covered/hidden by the dense vegetation on the pre-Haiyan image.

4.2 Field and laboratory work

In the field, the elevation of all dislocated clasts was measured using a Topcon HiPer Pro differential global positioning system (DGPS) with an altimetric accuracy of ±2 cm. Elevations were referenced to mean lower low water level (MLLW). The first field survey was carried out in February 2014, three months after the typhoon. A second field survey was conducted between 5 and 20 March 2015. Altogether 59 clasts with longest axes >1 m were documented in the field at site ESA (Fig. 1b). The clasts were classified as "transported", "not transported", or "possibly transported" during Haiyan based on vegetation cover, weathering patterns and color of rock surfaces, the freshness of buried plant debris, and satellite imagery. Five of the dislocated boulders (ESA 1, 5, 7–9) were studied in high detail. The original (pre-transport) position of ESA 1 and 5 was identified based on fresh scars in the carbonate platform and the equal pattern of coral branches exposed within the scarp and at the clasts' surface. The carbonate rock at the original position of ESA 7 and 9 appeared less weathered/karstified and has a significantly lighter color compared to surrounding platform sections, and a 5 cm high pedestal was documented at the pre-Haiyan position of ESA 9. The clasts' trajectories and transport distances were identified by tracing impact marks on the carbonate platform using a DGPS. The distribution of fresh percussion marks on the clasts' surface additionally gave evidence for their transport mode.

Two different approaches for calculating the clasts' volumes (V) were applied following the procedure described in a previous study (Engel and May, 2012): (i) a (length), b (width) and c (height) axes of the selected boulders were measured for conventional calculations of $V_{abc} = a \cdot b \cdot c$ using a measuring tape. (ii) Upper and lower vertices and edges were measured using a DGPS in order to calculate the V with high accuracy. The DGPS-measured point cloud was imported into a GIS (ESRI ArcGIS) and translated into 3D surfaces by computing triangulated areas between the GPS points. The boulder volume (V_{DGPS}) was then calculated by subtraction of the volume between the boulder's lower surface and the ground surface from the volume between the boulder's upper surface and the ground surface. Discrepancies between the two methods are shown in column V_{DGPS}/V_{abc} and represent the correction factor for V_{abc} values. V_{DGPS} and other emerging approaches such as terrestrial laser scanning (Hoffmann et al., 2013; Hoffmeister et al., 2014) or multi-view image measurement techniques (Khan et al., 2010; Terry et al., 2013; Gienko and Terry, 2014) are assumed to provide the best approximates of the real volume of the clasts. The clasts' bulk density (ρ_b) was calculated from five samples representative of the lithological composition of ESA 7 using the Archimedean principle (buoyancy in sea water) (Hughes, 1987).

Based on this and a previous study (Engel and May, 2012), best estimates of volume and weight of limestone boulders along tropical coasts are ~60% of V_{abc} on average. In addition to the dimensions indicated by the authors, we therefore give corrected volumes (V_{corr}) and weights (W_{corr}) for the largest clasts in literature for which transport during storms was directly observed (Table 1).

4.3 Modelling

By using Delft3D and Delft Dashboard software, a high-resolution storm surge model for the boulder site was created and nested into a coarser one, which provides the initial conditions at the open boundaries of the high-resolution model. While the built-in GEBCO (bathymetry) and SRTM (topography) data from Delft Dashboard was used for the coarse model (1 km spatial resolution), IFSAR data (topography) as well as a combination of nautical chart (near-shore bathymetry) and GEBCO (offshore bathymetry) data were used in the nested model. The different datasets were interpolated to the computational grid, resulting in a spatial resolution of 50 m. Further steps in model creation and details on boundary conditions can be found in Cuadra et al. (2014).

Wind forcing in Delft3D was based on a Wind Enhancement Scheme (WES) following Holland's model to generate the tropical cyclone wind field (Holland, 1980). A spiderweb file was generated using the JTWC best track data of Typhoon Haiyan which includes data about typhoon track, maximum sustained wind speed, and pressure field.

Tides may either reduce or add to the storm surge in the area. For relatively small coastal models such as the nested one presented here, the treatment of tidal forcing along the open boundaries is sufficient in generating the appropriate tidal motion. Tidal forcing in Delft3D was based on TPXO 7.2 Global Inverse Tide Model to acquire the phases and amplitudes for cells in the model.

In order to derive estimates of minimum flow velocities required to move the dislocated boulders, we applied the equations (initiation-of-motion criteria) of Nandasena et al. (2011). Equations differ based on transport modes. Values for input parameters include boulder axes (derived from field measurements), inclination of original boulder position (θ) (inferred from DGPS transects), density of sea water (ρ_w) and the boulder (ρ_s), boulder-specific coefficients of drag (C_d), ~~and~~ lift forces (C_l), and static bottom friction (μ).

5 Results

5.1 Block and boulder transport based on pre- and post-typhoon satellite images

The comparison of pre- and post-Haiyan satellite images (WV1 and 2) illustrate changes in the position of large inter- to supratidal clasts at our study site (Fig. 3) and at several further sections of the adjacent coastline (Fig. 4). At site ESA, the largest transported clasts are found in the intertidal zone along the landward margin of the 150 m wide Holocene lagoon (Figs 1b, 3a,b). ESA 9 was shifted shore-parallel by ~40 m along the upper intertidal to lower supratidal of the reef platform. ESA 7 was moved on the lower supratidal platform by ~30 m. Further north, on top of the gently inclined Pleistocene carbonate platform, vegetation (mostly coconut trees) is almost entirely removed in the post-Haiyan image (Figs 1b, 3b). Large clasts can be spotted on top of the platform at various locations, although in most cases their pre-Haiyan position remains unknown due to the dense vegetation cover in May 2013. A fresh scarp along the cliff edge at the transition from the carbonate platform to the Holocene lagoon was detected on the post-Haiyan satellite image. Dislocation of further clasts is inferred for the central part of the lagoon, on top of the Holocene reef platform (Figs 1b).

To the north and south of site ESA, several further clasts were shifted according to the pre- and post-Haiyan satellite images (Fig. 4a-d). Dislocation of large block-sized clasts were spotted some 500 m north of ESA, where two triangle-shaped blocks (with longest axis >4 and >5 m, respectively) were shifted on top of the Holocene reef platform; a distance of >240 m is inferred for the smaller one (Fig. 4b). In the omega-shaped bay south of ESA (Pook

Cove), just north of Tugnug Point, and in Nagaha Bay, numerous large clasts of pre-existing boulder fields changed position as well (Fig. 4c,d).

5.2 Field evidence – block and boulder fields in ~~E Samar~~Eastern Samar

Out of the 59 clasts (longest axes >1 m) documented at site ESA (Fig. 1b), 30 clasts showed clear signs of ~~subrecent~~ recent transport, and 13 clasts must have been transported by a previous event based on their mature vegetation cover. For 16 clasts, dislocation during Haiyan remains ambiguous.

At ESA, the largest clast found to be dislocated amounts to ~180 t (ESA 9: ~75 m³; 9.0x4.5x3.5 m³; Fig. 5a,b). Its main axis was slightly turned during transport and is now perpendicular to the shore. The pre-Haiyan location of ESA 9 shows a ~ 5 cm high pedestal which had formed below ESA 9 prior to dislocation in the intertidal zone of the reef platform (Fig. 5b). Its source is the receding cliff of the Pleistocene reef terrace. Another large boulder (ESA 7: ~30 m³; 5.3x3.0x2.9 m³; ~70 t; Fig. 5c) was found some 40 m northwest of ESA 9. Evidence for overturning and rolling of ESA 7 was found in the form of downward-facing and still living grass-patches, impact marks on the supratidal platform along its track, and fresh wood jammed under the rock (Fig. 6). In contrast, grass patches on top, a lack of impact marks at the surface, and a notch opening towards the base were documented for block ESA 9 and indicate sliding transport and no overturning.

Some 50 m to the north, numerous slab-shaped boulders were dislocated on top of the gently inclined Pleistocene carbonate platform. A boulder of ~23.5 t (ESA 5: ~10 m³; 4.0x2.8x1.7 m³; Fig. 6a,b) was quarried at 2 m MLLW from the cliff edge of the carbonate platform leaving a fresh scarp, which was detected on the post-Haiyan satellite image as well (see also sect. 5.1). It was transported vertically to 6 m MLLW by rolling or even saltation. Boulders of up to ~17 t (e.g. ESA 1; Fig. 5d) were moved upwards from 6.5 to 10 m MLLW, 2 m below the highest run-up marks (Fig. 1c). Downward-facing rock pools and grass patches, still living barnacles, roots and soil staining on the exposed former bottom side, snapped palm trees, and fresh wood jammed under the rocks were found for the clasts on top of the Pleistocene carbonate platform as well (Fig. 6). The pre-Haiyan vegetation was almost entirely devastated, and flood debris display the limit of highest run-up at 12 m MLLW. The platform is covered by a thick sheet of whitish reef-borne sand and gravel overlying a brownish top soil horizon developed in an older carbonate sand deposit.

5.3 Calculation of flow velocities for block and boulder transport

Blocks and boulders may be moved by fluid forces in the form of sliding, rolling, or saltation (e.g., Nandasena et al. 2011), depending on flow velocity, bottom friction as well as the clasts' shape and weight. Based on the pioneering contributions of Nott (1997, 2003), Nandasena et al. (2011) presented improved hydrodynamic equations for calculating estimates of minimum flow velocities (u) necessary for the initiation of coastal block and boulder motion by tsunamis and storms. The equation for the initial transport mode "sliding" of submerged or subaerial (e.g. ESA 9) clasts reads

$$u^2 \geq \frac{2 \cdot \left(\frac{\rho_s}{\rho_w} - 1\right) \cdot g \cdot c \cdot (\mu_s \cdot cos\theta + sin\theta)}{C_d \cdot \frac{c}{b} + \mu_s \cdot C_l} \qquad (1),$$

where ρ_s = density of the boulder = 2.4 g cm^{-3}; ρ_w = density of sea water = 1.02 g cm^{-3}; g = gravitational acceleration = 9.81 m s^{-2}; c = boulder's height (in all cases the boulder's shortest axis); b = boulder's width (in all cases the boulder's second longest axis); and ~~μ_s = coefficient of static friction = 0.7 (Nandasena et al. 2011);~~ θ = angle of the bed slope.~~; C_d = coefficient of drag = 1.95; b~~ We applied boulder-specific values for C_d = coefficient of drag (Table 2) by calculating boulder-specific shape factors (Corey, 1949) and taking the appropriate C_d ~~factors~~values from Fig. 3 in Helley (1969), as suggested by Normeets et al. (2004). ~~C_l = coefficient of lift = 0.178 (Nott 1997; Noormets et al. 2004).~~ For C_l = coefficient of lift, we used 0.178 according to previous studies (e.g., Nott 1997; Noormets et al. 2004). Finally, we adopted μ_s = coefficient of static friction = 0.7 according to Nandasena et al. (2011) and the values given for sand-covered limestone platforms in Goto et al. (2007) and Buckley et al. (2012) (Fig. 7, case 1). For each clast, flow velocities were additionally calculated with minimum C_l (0.05) and maximum μ_s (1.02) values provided in previous studies (Nott, 2003; Benner et al., 2010) (Fig. 7, cases 2–4). ~~For C_d = coefficient of drag, we used boulder-specific values (Table x) by calculating boulder-specific shape factors and taking the appropriate C_d factors from Fig. 3 in Helley (1969), as suggested by Normeets et al. (2004).~~ The equation for the initial transport mode "rolling/overturning" of submerged or subaerial clasts (e.g. ESA 7) reads

Formatiert: Nicht Hervorheben

Formatiert: Nicht Hervorheben

Formatiert: Nicht Hervorheben

Formatiert: Tiefgestellt

$$u^2 \geq \frac{2 \cdot \left(\frac{\rho_s}{\rho_w} - 1\right) \cdot g \cdot c \cdot \left(\cos\theta + \frac{c}{b} \cdot \sin\theta\right)}{C_d \cdot \frac{c^2}{b^2} + C_l} \qquad (2),$$

whereas the equation for the initial transport mode “saltation/lifting” of clasts in a joint-bounded scenario (e.g. ESA 5) is

$$u^2 \geq \frac{2 \cdot \left(\frac{\rho_s}{\rho_w} - 1\right) \cdot g \cdot c \cdot (\cos\theta + \mu_s \cdot \sin\theta)}{C_l} \qquad (3),$$

Accordingly, boulder ESA 7 requires minimum flow velocities of ~~5~~7.~~2~~6 m s^{-1} to initiate sliding transport and of ~~6~~8.~~2~~9 m s^{-1} to initiate rolling transport. For the largest block ESA 9, initiation of sliding transport requires ~~6~~7.~~3~~4 m s^{-1}, and flow velocities of ~~8~~9.~~3~~6 m s^{-1} would have been required for overturning (Fig. 7, case 1).

On top of the carbonate platform, flow velocities of 6.~~8~~7 m s^{-1} are necessary for the initial transport with overturning of ESA 1. For boulder ESA 5, which was quarried from the cliff edge (joint bounded boulder scenario) and must have experienced saltation and lifting during initial transport, flow velocities were calculated to ~~15.9~~16 m s-1. The boulder transport histogram shown in Fig. 7 illustrates the critical flow velocities necessary for the initiation of different transport modes of each investigated clast.

5.4 Storm surge and wave model

While previously published models with a spatial resolution of 2.5 km resulted in maximum significant wave heights of ≥15 m during Haiyan in deep water off Eastern Samar (Bricker et al., 2014; Fig. 3), maximum significant wave heights of ~4-5 m and ~5-6 m are inferred for site ESA and for Hernani, respectively, from the ~~here presented~~ Delft3D model presented in this study (Fig.8a). This is comparable to maximum significant wave heights inferred from recently published higher-resolution Delft3D models off the Holocene reef at Hernani (Bricker and Roeber, 2015).

Combining pressure- and wind-driven surge as well as wave setup, our coupled hydrodynamic and wave model results in slightly elevated maximum water levels (< 1 m above mean sea level, a.s.l.), and maximum flow velocities below 1.5 m s-1 (Fig. 8b,c) at site ESA during Haiyan. Flow velocities at Hernani and in Matarinao Bay already reach high~~est~~ values at 5~~.~~:30 a~~.~~m~~.~~ local time, while max. flow velocities at ESA are approached at ~8 a~~.~~m.~~.~~

Formatiert: Nicht Hervorheben

Formatiert: Nicht Hervorheben

Formatiert: Nicht Hervorheben

However, the modeled water levels are comparable to those inferred from previously published storm surge and FLO2D flood routing models (e.g., Bricker et al., 2014), where still water levels increase to a maximum of ~2.5 m a.s.l. along the Hernani coast and in Matarinao Bay, but remain <1 m a.s.l. at site ESA.

Most recently, the high-resolution model of Bricker and Roeber (2015) resulted in surge-related maximum still water levels of 4 m a.s.l. at Hernani and maximum flow speeds of ~3 m s-1 off the reef crest; however, flow speeds still rapidly decrease to <1.5 m s-1 on the reef platform and along the coastline, similar to the values presented here (Fig. 8b,c).

6 Discussion

6.1 Boulder transport and flow velocities inferred by inverse modelling

Based on field evidence, the interpretation of satellite images and the intensity of previous storms, the documented coarse clast transport can unambiguously be attributed to marine flooding during Haiyan. The size of individual clasts and in particular the dimensions of block ESA 9 (9.0x4.5x3.5 m³), in combination with the documented vertical and lateral transport distances, exceeds any existing literature account including the often-cited boulder at Sydney's Bondi Beach (Süssmilch, 1912; 6.1x4.9x3.0 m³), and clasts moved during TCs in Japan (Goto et al., 2011) and Jamaica (Khan et al., 2010) as well as during Atlantic winter storms (Williams and Hall, 2004; Regnauld et al., 2010; Cox et al., 2012) (Tables 1, 2). According to the pedestal found at its pre-Haiyan position, block ESA 9 was stationary for a considerable period of time prior to Typhoon Haiyan (cf. Matsukura et al., 2007).

The largest transported clasts on the intertidal platform (ESA 7 and 9) show a shore-perpendicular orientation of their longest axis (Fig. 3). Their transport direction, as can be traced by impact marks on the carbonate platform and bitemporal satellite image analysis, documents SE-NW-directed water currents (Fig. 3), coincid~~es~~ing with the modeled flow vectors in direct vicinity of site ESA (Fig. 8)~~ and, thus, with SE-NW-directed surge-accompanying water currents (Fig. 3)~~. In contrast, for the rather flat boulders on top of the upper carbonate platform, the orientation of their longest axis is oblique to shore-parallel (Fig. 3), suggesting alignment to approaching superimposed storm waves and/or deflection of water currents on top of the reef platform by the ~2 m high cliff.

Compared to previously published low resolution models ~~previous studies of (~~Bricker et al., ~~(~~2014; Fig. 3) and to wave heights generally expected during catastrophic typhoons such as Haiyan, our model apparently results in underestimated maximum significant wave heights offshore of Eastern Samar. These discrepancies may particularly be explained by the different typhoon track data used in this study, with 1-min sustained winds implemented in the JTWC track. However, the timing of maximum significant wave heights in our model is generally in agreement with the timing of the catastrophic flooding at Hernani, video captured at ~6 am PHT. According to our model, highest waves developed at ~5:~~1~~20 am (depicted in Fig. 8a) and lasted until ~6 am PHT, while highest flow velocities at site ESA (due to pressure- and wind-driven setup) occurred delayed (Fig. 8b,c). This is corroborating ~~with~~ results presented by Roeber and Bricker (2015), stating that modeled offshore wave heights dropped rapidly after 6 am PHT, while pressure- and wind-induced setup ~~continued to show high values~~remained high.

However, despite the discrepancies and similarities mentioned above, f~~F~~low velocities modelled with Delft3D in this study and in all previous studies are insufficient to account for the transport of the documented clasts (Fig. 8; see also Bricker et al., 2014; Bricker and Roeber, 2015). For the rather spherical boulder ESA 7, a rolling transport mode was inferred from the field observations requiring at least ~~6~~8.~~2~~9 m s^{-1} for the initiation of movement (Fig. 7, case 1) when assuming no vertical component in the transport track (θ = 0~~,~~.5). In contrast, a sliding transport mode due to flow velocities higher than ~~~6~~7.~~3~~4 m s^{-1} but below ~~~8~~9.~~3~~6 m s^{-1} is assumed for dislocation of the largest block ESA 9 since no signs of overturning were observed.

While these flow velocities are based on boulder-specific C_d values, uncertainties remain ~~regarding the~~ in terms of realistic (boulder- and site-specific, respectiv~~l~~ely) values ~~given~~ for C_l and μ_s~~, the latter one potentially being very site-specific as well~~. In addition to μ_s = 0.7~~, as applied in~~ (Noormets et al.~~ (~~, 2004~~),~~; Paris et al.~~ (~~, 2010~~),~~; ~~and~~ Nandasena et al.~~ (~~, 2011~~),~~) values between 0.6 or 0.65–0.8 (Goto et al., 2007; Benner et al.; 2010; Buckley et al., 2012) or between 0.82–1.02 (Nott, 2003; based on empirical studies of Fukui et al., 1963) have been suggested, ~~in most cases within~~most of them in the context of sand-covered limestone platforms. While changes of the calculated flow velocities for sliding transport mode are negligible with μ_s = 0.6, ~~However, only the application of values given by Nott (2003) result in n~~Notable changes ~~of the calculated flow velocities for sliding transport mode~~ are

Formatiert ... [1]

Formatiert ... [2]

Formatiert: Schriftart: (Standard) Times New Roman, 12 Pt., Schriftfarbe: Schwarz, Hochgestellt

Formatiert ... [3]

Formatiert: Schriftart: (Standard) Times New Roman, 12 Pt., Schriftfarbe: Schwarz, Hochgestellt

Formatiert ... [4]

Formatiert: Schriftart: (Standard) Times New Roman, 12 Pt., Schriftfarbe: Schwarz, Hochgestellt

Formatiert: Schriftart: (Standard) Times New Roman, 12 Pt., Schriftfarbe: Schwarz

Formatiert ... [5]

particularly recognised when applying the max~~-~~imum values given by Nott (2003)~~,~~: with μ_s = 1.02, up to 1.9 m s^{-1} higher ~~changing by the order of 0.2~~ flow velocities are necessary to initiate sliding of ESA 7 and ESA 9 ~~m/s~~(Fig. 7, cases 2 and 4). ~~As to~~For C_l, ~~every~~realistic values range between 0.05 and 0.2 ~~may be realistic~~ according to Benner et al. (2010), with 0.2 being very close to the one used in case 1 of this study (Fig. 7) and in previous studies (0.178; Nott, 2003; Noormets et al., 2004; Paris et al., 2010; Nandasena et al., 2011). ~~The application of Benner's~~The minimum value for C_l (0.05) results in slightly increased ~~(i.e. 0.5-0.7< 0.9 m s^{-1} m/s higher)~~ flow velocities (i.e. < 0.9 m s^{-1} higher) for rolling/sliding of ESA 7 and 9 (Fig. 7, cases 3 and 4), and considerably increased ~~(up to ~20 m s^{-1})~~ flow velocities (up to ~20 m s^{-1}) for saltation/lifting ~~(up to ~20 m/s)~~.

Consequently, the ~~presented~~ flow velocities calculated for case 1 represent conservative (i.e., minimum) values, and flow speeds at this study site most probably exceeded ~~6~~8.9~~.3~~ m s^{-1} but remained below ~~8~~9.~~3~~ 6 m s^{-1}. Calculated flow velocities for these clasts are thus in the range of or even higher than those inferred for recent major tsunamis at the coast (Fritz et al., 2006, 2012).

Based on the applied formula, quarrying of ESA 5 from the cliff edge, as documented by the field survey, requires flow velocities of at least ~~~15.9~~16 m s-1 (Fig. 7). Since these flow velocities would have caused rolling transport of ESA 9, ambiguities remain at least for the values resulting from the joint-bounded boulder scenario, which tends to ~~result in~~ significant~~ly~~ ~~overestimated~~ overestimation ~~values~~ (Switzer and Burston, 2010; Etienne, 2012). Discrepancies may for instance be related to the overestimation of strain forces between the block and the strongly karstified reef body, or to the underestimation of the waves' impact and lift forces approaching the cliffs and their associated jets (Hansom et al., 2008). However, flow velocities of ~~7~~8.~~1~~ 2 m s^{-1} are required for the subsequent rolling transport of ESA 5, which is in agreement with the flow velocities inferred from ESA 7 and 9. Against the background of previously published models (Bricker and Roeber, 2015; Roeber and Bricker, 2015) and the modelled low flow velocities presented here, it is apparent that hydrodynamic processes have to be considered for the dislocation of the ESA clasts, which are beyond storm surge and incident waves.

Formatiert ... [6]
Formatiert: Hochgestellt
Formatiert ... [7]
Formatiert: Hochgestellt
Formatiert ... [8]
Formatiert: Hochgestellt
Formatiert ... [9]
Formatiert ... [10]
Formatiert ... [11]
Formatiert ... [12]
Formatiert: Hochgestellt
Formatiert ... [13]

6.2 Origin of exceptional flooding pattern

A very high velocity of the typhoon over the NW Pacific (32 km h^{-1}), an unusually warm subsurface ocean layer, and a long travel distance over the open ocean (3000 km) (Normile, 2013; Pun et al., 2013) probably provided the momentum for Hayian's exceptional storm surge. For the Leyte Gulf and in particular San Pedro Bay off Tacloban, Mori et al. (2014) conclude that amplification of storm surge-induced water levels was due to seiches, also provoking the specific inundation pattern of distinct flooding pulses observed by residents.

In contrast, wind- and pressure-driven storm surge along the SE Samar coast is believed to not having exceeded ~1 m due to the steep slope off the coast, but setup by breaking waves locally induced water levels of up to ~2.5 m such as on top of the broad Holocene reef platforms (see also Bricker et al., 2014) or even 4 m at Hernani (Bricker and Roeber, 2015). However, in all phase-averaged (e.g., Delft3D/SWAN-based) coupled wave and storm surge models considering breaking-wave setup, including the here-presented one, modeled flow velocities on top and landward of the reef platform remain < 1.5 m s-1 (cf. Bricker and Roeber, 2015) and thus remarkably below those required for the clast transport documented at ESA during Haiyan.

To explain the surprisingly high inundation levels in SE Samar (Tajima et al., 2014) and the bore-like coastal flooding captured at Hernani (Mas et al., 2015), Bricker et al. (2014) hypothesized that infragravity waves (such as surf beat) (Munk, 1950) were caused by non-linear wave interactions with the reef, which are not resolved by the existing Delft 3D and SWAN models. A Haiyan-related meteo-tsunami can be excluded due to a lack of bathymetric conditions with suitable resonance properties. Most recently, based on models simulating wave transformation over shallow fringing reefs using Boussinesq-type equations, Shimozono et al. (2015) and ~~Bricker and~~ Roeber and Bricker ~~–~~(2015) confirmed that the extreme run-ups and the bore-like flooding pattern in ~~E Samar~~Eastern Samar must be explained by strong coupling of sea swells and infragravity waves with periods of ~~several minutes~~ > 1 minute, which may have experienced excitation by resonances with the fringing reef (Péquignet et al., 2009). These models inferred flow speeds of up to 6 m s-1 at the video site in Hernani, which is in good agreement with the flow speeds derived from (i) the video footage at Hernani onshore (Bricker and Roeber, 2015); and (ii) initiation-of-motion criteria of the coarse-clast record presented in this study. Since pressure- and wind-induced setup ~~and max. offshore wave heights~~ occurred delayed with respect to max~~.~~imum offshore wave heights (Roeber and Bricker, 2015; Fig. 8c), the most destructive ~~waves~~infragravity waves developed only within a short time window, before offshore wave heights rapidly dropped after ~6 a~~.~~m~~.~~ PHT (Roeber and Bricker, 2015).

Surf beat resulting in pulses of elevated water depths and flow velocities is thus assumed as the driving process for the transport of the investigated boulders some 4 km north of the Hernani video site. Although the NW-directed longshore currents, as documented by the shore-parallel trajectories of ESA 7 and 9, agree with the modeled flow vectors of wind- and pressure-driven storm surge, surf beat-generated currents deviating from a shore-normal direction, and/or the ~~It however remains open how and to which extend infragravity waves also cause longshore currents, which are inferred by the shore parallel trajectory of the clasts.~~ ~~D~~deflection of these currents along the cliffs must be assumed for the study area ~~coast may potentially play a role in the direction of infragravity wave-driven water currents on top of the reef platform.~~ . However, regardless of the mechanisms responsible for the exceptional coastal flooding pattern, the sedimentary findings presented here give striking evidence of very high run-up and strong wave- and surge-accompanying sustained currents along the coast of SE Samar during Supertyphoon Haiyan. They were capable to transport block-sized clasts over horizontal distances of up to ~40 m and to produce spatially randomized clast distributions, both which are often associated with tsunami deposition.

7 Conclusions

Based on their SE–NW trajectory and a surge-perpendicular orientation of their longest axis (Fig. 3), we conclude that the exceptional flooding pattern, caused by wave setup and infragravity waves, induced the transport of the largest clasts rather than the high breaking waves alone. This is in contrast to many previous observations and descriptions of storm-moved boulders, which are defined to be “wave-transported” (Table 1). However, the shore-parallel orientation of the slab-shaped boulders on top of the carbonate platform may suggest that superimposed waves, having reached heights of more than 5 m (Bricker et al., 2014), contributed to their trajectory as well. The remarkable flooding pattern video-captured at Hernani thus affected a wider coastal section, i.e. ~5 km to the north, and was not restricted to special boundary conditions in urbanized areas such as sea wall structures at Hernani.

Supported by post-typhoon survey reports (Bricker et al., 2014; Tajima et al., 2014), recent wave models (Shimozono et al., 2015), eyewitness accounts and video footage (Mas et al.,

Formatiert: Nicht Hervorheben

Formatiert: Nicht Hervorheben

Formatiert: Nicht Hervorheben

Formatiert: Nicht Hervorheben

Formatiert: Nicht Hervorheben

Formatiert: Nicht Hervorheben

Formatiert: Nicht Hervorheben

Formatiert: Nicht Hervorheben

2015; Bricker and Roeber, 2015), our findings suggest that a variety of hydrodynamic processes related to TC landfall must be considered when interpreting boulder deposits along coasts. These processes may include, in addition to ~~ordinary~~incident (~~though~~ potentially very high) gravity waves and (or on top of) pressure- and wind-driven storm surge, meteo-tsunamis or seiches (Mori et al., 2014), and infragravity waves with periods of up to several minutes. The ~~resulting~~ sustained high-velocity coastal flooding resulting from these infragravity waves, in combination with inundation depths of several metres, is capable of transporting clasts similar to palaeo-deposits commonly related to tsunamis. This is in agreement with theory-based conclusions of Weiss (2012) that both tsunamis and storms may shift clasts of comparable sizes. Our conclusions have important implications for the interpretation of coastal block and boulder deposits and numerical simulations of their transport in similar settings. Where storms have previously been ruled out to be the cause of the dislocation and transport of very large clasts based on their dimensions, the geological legacy of Haiyan prompts the need for a careful reconsideration of possible storm-related transport.

Author contributions

S.M.M., D.B., M.E., M.R. and H.B. contributed to field and lab work. S.M.M., D.B., M.E., and H.B. designed the study and interpreted the data. Modelling was done by C.C., A.M.F.L., J.S. and J.K.S. Finally, S.M.M., D.B. and M.E. wrote the manuscript.

Acknowledgements

Financial support for the research is granted by the Faculty of Mathematics and Natural Sciences, University of Cologne (UoC), and a UoC Postdoc Grant. Invaluable logistic support was provided by Karen Tiopes and Verna Vargas (Department of Tourism, Leyte Branch). Kirstin Jacobson is acknowledged for language editing. Mark A.C. Bahala, Lia A.L. Gonzalo (both Project NOAH), Eva Quix (UoC), and Bastian Schneider (German International Cooperation [GIZ]) kindly supported boulder mapping. We are very appreciative of the great hospitality considering the situation left by the disaster and of first-hand insights by local interviewees throughout the Visayas archipelago.

References

Algué, J.: El baguio de Samar y Leyte, 12-13 de octubre de 1897, Marty, 1898.

Barrier, E., Huchon, P., and Aurelio, M.: Philippine fault: a key for Philippine kinematics. Geology, 19, 32–35, 1991.

Benner, R., Browne, T., Brückner, H., Kelletat, D. and Scheffers, A.: Boulder Transport by Waves: Progress in Physical Modelling. Zeitschrift für Geomorphologie N.F., 54, Suppl. 3, 127–146, 2010.

Boyson, H.: Photo taken and provided by Henry Boyson. http://www.panoramio.com/photo/82283313?source=wapi&referrer=kh.google.com (last access: 23 Mar 2014), no date.

Bricker, J. and Roeber, V.: Mechanisms of damage during Typhoon Haiyan: storm surge, waves, and "tsunami-like" surf beat, E-proceedings of the 36th IAHR World Congress, 28 June–3 July, 2015, The Hague, the Netherlands, 2015.

Bricker, J., Takagi, H., Mas, E., Kure, S., Adriano, B., Yi, C., and Roeber V.: Spatial variation of damage due to storm surge and waves during Typhoon Haiyan in the Philippines, Journal of the Japan Society of Civil Engineers, Series B2, 70 (2), 231–235, 2014.

Buckley, M. L., Wei, Y., Jaffe, B. E. and Watt, S. G.: Inverse modeling of velocities and inferred cause of overwash that emplaced inland fields of boulders at Anegada, British Virgin Islands, Natural Hazards, 63, 133–149, 2012.

Cass, L.: Exploding The Myth – The Big Rock. The Bondi View 7, http://www.cyberbondi.com.au/v3/bondiview_1.html (last access: 23 Mar 2014), 2002.

Corral, A., Ossó, A., and Llebot, J.E.: Scaling of tropical-cyclone dissipation, Nature Physics, 6, 693–696, 2010.

Corey, A. T.: Influence of shape on fall velocity of sand grains. Unpublished M~~s~~Sc thesis, Colorado A&M College, 102 pp., 1949.

Formatiert: Englisch (USA)

Feldfunktion geändert

Formatiert: Schriftart: 12 Pt., Schriftfarbe: Schwarz

Cox, R., Zentner, D. B., Kirchner, B. J., and Cook, M. S.: Boulder ridges on the Aran Islands (Ireland): Recent movements caused by storm waves, not tsunamis, Journal of Geology, 120, 249–272, 2012.

Cuadra, C., Biton, N. I., Cabacaba, K. M., Santiago, J., Suarez, J. K., Lapidez, J. P., Lagmay, A. M. F., and Malano, V.: Development of Inundation Map for Bantayan Island, Cebu Using Delft3D-Flow Storm Surge Simulations of Typhoon Haiyan, NOAH Open-File Reports, 3, 37–44, 2014.

Engel, M. and May, S. M.: Bonaire's boulder fields revisited: Evidence for Holocene tsunami impact on the Leeward Antilles, Quaternary Science Reviews, 54, 126–141, 2012.

Etienne, S.: Marine inundation hazards in French Polynesia: geomorphic impacts of Tropical Cyclone Oli in February 2010, Geological Society, London, Special Publications, 361, 21–39, 2012.

Etienne, S., Buckley, M., Paris, R., Nandasena, A. K., Clark, K., Strotz, L., Chagué-Goff, C., Goff, J., and Richmond, B.: The use of boulders for characterizing past tsunamis: lessons from the 2004 Indian Ocean and 2009 South Pacific tsunamis, Earth-Science Reviews, 107, 76–90, 2011.

Felton, E. A. and Crook, K. A. W.: Evaluating the impacts of huge waves on rocky shorelines: an essay review of the book 'Tsunami – The Underrated Hazard', Marine Geology, 197, 1–12, 2003.

Fritz, H. M., Borrero, J. C., Synolakis, C. E., and Yoo, J.: 2004 Indian Ocean tsunami flow velocity measurements from survivor videos, Geophysical Research Letters, 33, L24605, 2006.

Fritz, H. M., Blount, C. D., Thwin, S., Kyaw Thu, M., and Chan, N.: Cyclone Nargis storm surge in Myanmar, Nature Geoscience, 2, 448–449, 2009.

Fritz, H. M., Phillips, D. A., Okayasu, A., Shimozono, T., Liu, H., Mohammed, F., Skanavis, V., Synolakis, C. E., and Takahashi, T.: The 2011 Japan tsunami current velocity measurements from survivor videos at Kesennuma Bay using LiDAR, Geophysical Research Letters, 39, L00G23, 2012.

Fukui, Y.; Nakamura, M., Shiraishi, H. and Sasaki,Y.: Hydraulic study on tsunami: Coastal Engineering in Japan, 6, 67–82, 1963.

Gensis, N.: Eyewitness footage of Typhoon Haiyan washing house away; video taken at Hernani, Eastern Samar, at 6 am, 8th Nov 2013 by Nickson Gensis, Plan Philippines Community Development Worker, http://www.youtube.com/watch?v=rS0gv4Xbw7w (last access 06 Jun 2014), 2013.

Gienko, G. A., and Terry, J. P.: Three-dimensional modeling of coastal boulders using multi-view image measurements. Earth Surface Processes and Landforms, 39, 853–864, 2014.

Google Earth/Digital Globe: Bondi Beach, Australia. 33.893723°S, 151.282965°W, Eye alt 220 m. Image taken on March 11, 2007, http://www.earth.google.com (last access 25 March 2014), 2014.

Goto, K., Chavanich, S. A., Imamura, F., Kunthasap, P., Matsui, T., Minoura, K., Sugawara, D. and Yanagisawa, H.: Distribution, origin and transport process of boulders deposited by the 2004 Indian Ocean tsunami at Pakarang Cape, Thailand, Sedimentary Geology, 202, 821–837, 2007.

Goto, K., Miyagi, K., Kawamata, H., and Imamura, F.: Discrimination of boulders deposited by tsunamis and storm waves at Ishigaki Island, Japan, Marine Geology, 269, 34–45, 2010.

Goto, K., Miyagi, K., Kawana, T., Takahashi, J., and Imamura, F.: Emplacement and movement of boulders by known storm waves—Field evidence from the Okinawa Islands, Japan, Marine Geology, 283, 66–78, 2011.

Hansom, J. D., Bartrop, N. D. P., and Hall, A. M.: Modelling the processes of cliff-top erosion and deposition under extreme storm waves, Marine Geology, 253, 36–50, 2008.

Helley, E. J.: Field measurement of the initiation of large bed particle motion in blue creek near Klamath, California, U.S. Geological Survey Professional Paper, 562-G, 1969.

Hoffmann, G., Reicherter, K., Wiatr, T., Grützner, C., and Rausch, T.: Block and boulder accumulations along the coastline between Fins and Sur (Sultanate of Oman): tsunamigenic remains? Natural Hazards, 65, 851–873, 2013.

Hoffmeister, D., Ntageretzis, K., Aasen, H., Curdt, C., Hadler, H., Willershäuser, T., Bareth, G., Brückner, H., and Vött, A.: 3D model-based estimations of volume and mass of high-

Formatiert: Englisch (USA)

Formatiert: Englisch (USA)

Formatiert: Englisch (USA)

Formatiert: Englisch (USA)

energy dislocated boulders in coastal areas of Greece by terrestrial laser scanning, Zeitschrift für Geomorphologie N.F., 58, Suppl.~~, 58(~~ 3~~)~~, 115–135, 2014.

Holland, G. J.: An analytic model of the wind and pressure profiles in hurricanes, Monthly Weather Review, 108, 1212–1218, 1980.

Hughes, T. P.: Skeletal density and growth form of corals, Marine Ecology Progress Series, 35, 259–266, 1987.

IRIDeS (International Research Institute of Disaster Science): Initial Report of IRIDeS fact-finding mission to Philippines, TOHOKU University, 2014.

JTWC: 1984 Annual Tropical Cyclone Report. U. S. Naval Oceanography Command Center/Joint Typhoon Warning Center, Guam, http://www.usno.navy.mil/NOOC/nmfc-ph/RSS/jtwc/atcr/1984atcr.pdf (last access 24 Aug 2014), 1985.

JTWC: 2013 Annual Tropical Cyclone Report. U. S. Naval Oceanography Command Center/Joint Typhoon Warning Center, Guam, http://www.usno.navy.mil/NOOC/nmfc-ph/RSS/jtwc/atcr/2013atcr.pdf (last access 29 Apr 2015), 2014.

Khan, S., Robinson, E., Rowe, D.-A., and Coutou, R.: Size and mass of shoreline boulders moved and emplaced by recent hurricanes, Jamaica, Zeitschrift für Geomorphologie N.F., 54, Suppl.~~, 54(~~3~~)~~, 281–299, 2010.

Komar, P. D., and Reimers, C. E.: Grain Shape Effects on Settling Rates, Journal of Geology, 86, 193~~–~~–209, 1978.

Lagmay, A.M.F., Agaton, R.P., Bahala, M.A., Briones, J.B.L.T., Cabacaba, K.M.C., Caro, C.V.C., Dasallas, L.L., Gonzalo, L.A.L., Ladiero, C.N., Lapidez, J.P., Mungcal, M.T.F., Puno, J.V.R., Ramos, M.M.A.C., Santiago, J., Suarez, J.K., and Tablazon, J.P.: Devastating storm surges of Typhoon Haiyan, International Journal of Disaster Risk Reduction, 11, 1–12, 2015.

Lapidez, J.P., Tablazon, J., Dasallas, L., Gonzalo, L.A., Cabacaba, K.B., Ramos, M.M.A., Suarez, J.K., Santiago, J., Lagmay, A.M.F., and Malano, V.: Identification of storm surge vulnerable areas in the Philippines through the simulation of Typhoon Haiyan-induced storm surge levels over historical storm tracks, ~~–~~Natural Hazards and Earth System Sciences, 15, 1473–1481, 2015.

~~Natural Hazards and Earth System Sciences Discussions, 3, 919–939, 2015.~~

Lorang, M. S.: A wave-competence approach to distinguish between boulder and megaclast deposits due to storm waves versus tsunamis, Marine Geology, 283, 90–97, 2011.

Maeda, Y., Siringan, F., Omura, A., Berdin, R., Hosono, Y., Atsumi, S., and Nakamura, T.: Higher-than-present Holocene mean sea levels in Ilocos, Palawan and Samar, Philippines, Quaternary International, 115–116, 15–26, 2004.

Maragos, J. E., Baines, G. B. K., and Beveridge, P. J.: Tropical Cyclone Bebe creates a new land formation on Funafuti Atoll, Science, 181, 1161–1164, 1973.

Mas, E., Bricker, J., Kure, S., Adriano, B., Yi, C., Suppasri, A., and Koshimura, S.: Field survey report and satellite image interpretation of the 2013 Super Typhoon Haiyan in the Philippines, Natural Hazards and Earth System Sciences, 15, 805–816, 2015.

Matsukura, Y., Maekado, A., Aoki, H., Kogure, T., and Kitano, Y.: Surface lowering rates of uplifted limestone terraces estimated from the height of pedestals on a subtropical island of Japan, Earth Surface Processes and Landforms, 32, 1110–1115, 2007.

Mori, N., Kato, M., Kim, S., Mase, H., Shibutani, Y., Takemi, T., Tsuboki, K., and Yasuda, T.: Local amplification of storm surge by Super Typhoon Haiyan in Leyte Gulf, Geophysical Research Letters, 41(14), 5106–5113, 2014.

Munk, W. H.: Origin and generation of waves, Coastal Engineering Proceedings, 1, 1–4.

Nandasena, N. A. K., Paris, R., and Tanaka, N.: Reassessment of hydrodynamic equations: Minimum flow velocity to initiate boulder transport by high energy events (storms, tsunamis), Marine Geology, 281, 70–84, 2011.

NDRRMC, Republic of the Philippines, National Disaster Risk Reduction and Management Council: SitRep No. 09 re Effects of Tropical storm BASYANG (KAJIKI), http://www.ndrrmc.gov.ph/index.php?option=com_content&view=article&id=1143:preparations-for-tropical-storm-qbasyangq-kajiki (last access 31 May 2014), 2014.

Normile, D.: Clues to supertyphoon's ferocity found in the Western Pacific, Science, 342, 1027, 2013.

Noormets, R., Crook, K. A. W., and Felton, E. A.: Sedimentology of rocky shorelines: 3. Hydrodynamics of megaclast emplacement and transport on a shore platform, Oahu, Hawaii, Sedimentary Geology, 172, 41–65, 2004.

Nott, J.: Extremely high-energy wave deposits inside the Great Barrier Reef, Australia: determining the cause – tsunami or tropical cyclone, Marine Geology, 141, 193–207, 1997.

Nott, J.: Waves, coastal boulder deposits and the importance of the pre-transport setting, Earth and Planetary Science Letters, 210, 269–276, 2003.

Omura, A., Maeda, Y., Kawana, T., Siringan, F. P., and Berdin, R. D.: U-series dates of Pleistocene corals and their implications to the paleo-sea levels and the vertical displacement in the Central Philippines, Quaternary International, 115–116, 3–13, 2004.

PAGASA: Storm surge occurrences during the passage of Typhoon Yolanda on November 8, 2013 in selected areas of Leyte and Samar, Report of PAGASA Stride team 2014, 2014.

Péquignet, A. C. N., Becker, J. M., Merrifield, M. A., and Aucan, J.: Forcing of resonant modes on a fringing reef during tropical storm Man-Yi, Geophysical Research Letters, 36, L03607, 2009.

Philippine Weather Bureau: The Typhoon of Samar, Leyte and Panay, November 24 and 25, 1912, Meteorological Bulletin of the Philippine Weather Bureau, November 1912, 391–402, 1912.

Pun, I.-F., Lin, I.-I., and Lo, M.-H.: Recent increase in high tropical cyclone heat potential area in the Western North Pacific Ocean, Geophysical Research Letters, 40, 4680–4684, 2013.

Ramos, N. and Tsutsumi, H.: Evidence of large prehistoric offshore earthquakes deduced from uplifted Holocene marine terraces in Pangasinan Province, Luzon Island, Philippines, Tectonophysics, 495, 145–158, 2010.

Regnauld, H., Oszwald, J., Planchon, O., Pignatelli, C., Piscitelli, A., Mastronuzzi, G., and Audevard, A.: Polygenetic (tsunami and storm) deposits? A case study from Ushant Island, western France, Zeitschrift für Geomorphologie N.F, ~~Suppl., ~~54, Suppl. ~~(~~3~~)~~, 197–217, 2010.

Richmond, B. M., Watt, S., Buckley, M., Jaffe, B., Gelfenbaum, G., and Morton, R. A.: Recent storm and tsunami coarse-clast deposit characteristics, southeast Hawaii, Marine Geology, 283, 79–89, 2011.

Scheffers, S. R., Scheffers, A., Kelletat, D., and Bryant, E. A.: The Holocene paleo-tsunami history of West Australia, Earth and Planetary Science Letters, 270, 137–146, 2008.

Scicchitano, G., Monaco, C., and Tortorici, L.: Large boulder deposits by tsunami waves along the Ionian coast of south-eastern Sicily (Italy), Marine Geology, 238, 75–91, 2007.

Shimozono, T., Tajima, Y., Kennedy, A. B., Nobuoka, H., Sasaki, J., and Sato, S.: Combined infragravity wave and sea-swell runup over fringing reefs by super typhoon Haiyan, Journal of Geophysical Research: Oceans, 120, 4463–4486, 2015.

Süssmilch, C. A.: Note on some recent marine erosion at Bondi, Journal Proceedings of the Royal Society of New South Wales, 46, 155–158, 1912.

Switzer, A. D. and Burston, J. M.: Competing mechanisms for boulder deposition on the southeast Australian coast, Geomorphology, 114, 42–54, 2010.

Tajima, Y., Yasuda, T., Pacheco, B. M., Cruz, E. C., Kawasaki, K., Nobuoka, H., Miyamoto, M., Asano, Y., Arikawa, T., Ortigas, N. M., Aquino, R., Mata, W., Valdez, J., and Briones, F.: Initial report of JSCE-PICE joint survey on the storm surge disaster caused by Typhoon Haiyan, Coastal Engineering Journal, 56, 1450006, 2014.

Terry, J., Lau, A. Y. A., and Etienne, S.: Reef-Platform Coral Boulders – Evidence for High-Energy Marine Inundation Events on Tropical Coastlines, Springer, New York, 2013.

Traveglia, C., Baes, A. F., and Tomas, L. M.: Geology of Samar, Manila, 1978.

Verhoef, P. N. W.: Abrasivity of Hawkesbury Sandstone (Sydney, Australia) in relation to rock dredging, Quarterly Journal of Engineering Geology and Hydrogeology, 26, 5–17, 1993.

Weiss, R.: The mystery of boulders moved by tsunamis and storms, Marine Geology, 295–298, 28–33, 2012.

Weiss, R. and Bourgeois, J.: Understanding Sediments—Reducing Tsunami Risk, Science, 336, 1117–1118, 2012.

Williams, D. M. and Hall, A. M.: Cliff-top megaclast deposits of Ireland, a record of extreme waves in the North Atlantic—storms or tsunamis? Marine Geology, 206, 101–117, 2004.

Tables

Table 1: Boulder axes, volume and weight of very large storm-transported clasts from literature documented by eyewitnesses or remote sensing. Uncorrected and tentatively corrected volumes (V_{abc}, V_{corr}) and weights (W_{abc}, W_{corr}) are given using a correction factor of 0.6 (0.8 for the rather cubic boulder at Bondi [Boyson, no date; Google Earth/Digital Globe, 2014]). T_l = lateral transport; T_v = vertical transport; ρ_b = bulk density. The displacement of the above indicated clasts occurred due to direct storm wave impact. For the block at Bondi Beach the original source gives a weight of "about 235 t" (Süssmilch, 1912, p. 155), whereas multiplication of axes and local rock density of c. 2.35 g · cm^{-3} (Süssmilch, 1912; Verhoef, 1993) reveals only 211 metric tons. Furthermore, questions about the reliability of the report on the storm wave transport in 1912 have been raised, citing pre-1912 photographs of the boulder in its present position (Cass, 2002; Scheffers et al., 2008).

Site	ρ_b (g · cm^{-3})	T_l (m)	T_v (m)	Dimensions (m)			Volume (m³)		Weight (t)		Remarks and sources
				a-axis	b-axis	c-axis	V_{abc}	V_{corr}	W_{abc}	W_{corr}	
Bondi Beach, Sydney (Australia)	2.35	50	-	6.1	4.9	3.0	89.7	71.7	211	169	Wave-transported during storm in 1912 (Süssmilch, 2012); often cited as an example for largest coastal boulder dimensions observed to have been moved during a storm (Felton and Crook, 2003; Switzer and Burston, 2010; Terry et al., 2013); values of dimensions and ρ_b were taken from the original source (Süssmilch, 1912); a correction factor of 0.8 derived from recent photography (Boyson, no date; Google Earth/Digital Globe, 2014) of the boulder was applied for calculation of V_{corr}
Kudaka Island (Japan)	2.01	29	-	7.2	5.8	1.4	<63	37.2	127	74.4	Wave-transported onto the intertidal reef platform during typhoon 6123 in 1961 based on an eyewitness report (Goto et al., 2011)
Okinawa Island (Japan)	N/A	3	-	5.0	5.0	2.5	N/A	N/A	94	56.4	Wave-transported; moved by waves of typhoon 9021 on a 15 m high cliff-top in 1990 based on direct observations (Goto et al., 2011)
Manchinoeal (Jamaica)	2.05	2	-	N/A	N/A	N/A	N/A	36.2	N/A	79.7	Uplifted 2 m on a 12 m high cliff and moved 55 m inland; dislocation was documented after Hurricane Dean 2007; given dimensions are reliable and derive from multi-view image measurement (Khan et al., 2010)
Funafuti Atoll (Tuvalu)	N/A	N/A	N/A	7.0	N/A	N/A	N/A	N/A	N/A	N/A	Wave-transported; moved and incorporated into a newly created rampart of coral rubble at the edge of a reef flat during cyclone Bébé in 1972 (Maragos et al., 1973)
Inisheer, Aran Islands (Ireland)	2.60	N/A	2	N/A	N/A	N/A	N/A	N/A	84	50.4	Wave-transported; moved onto a 2 m high limestone platform during a storm in 1941; larger blocks are reported within the boulder ridges, but their dislocation by storms has not been witnessed (Williams and Hall, 2004)
Inishmaan, Aran Islands (Ireland)	2.60	Several metres	-	11.5	4.0	0.65	29.9	17.9	78	46.8	Wave-transported; tabular boulder moved several metres laterally on a 17 m high cliff top during a storm in 1991 (Cox et al., 2012) based on a local eyewitness; incorporated in a boulder ridge
Ushant Island, Brittany (France)	2.70	Several metres	-	4.0	3.4	1.7	23.1	13.9	62.4	37.5	Wave-transported; boulder rafted in the intertidal zone for several metres during a storm in 2008 based on a post-storm survey (Regnauld et al., 2010)

1

Table 2: Boulder axes, volume and weight of most important clasts at site ESA, ~~E Samar~~Eastern Samar. T_l = lateral transport; T_v = vertical transport; ρ_b = bulk density. ~~*~~ a – V_{abc} of ESA 9 was corrected to V_{DGPS} using a conservative value of 0.6, which was empirically calculated for the similar-shaped boulder ESA 7; b – Corey shape factor and appropriate C_d values according to Corey (1949), Helley (1969: Fig. 3) and Koman and Reimers (1978).

Formatiert: Tiefgestellt

Boulder	ρ_b (g · cm^{-3})	T_l (m)	T_v (m)	Dimensions (m)			Volume (m³)		Weight (t)		V_{DGPS}/ V_{abc}	Corey shape factor = $c/\sqrt{ab}$ and C_d[b]	Remarks
				a-axis	b-axis	c-axis	V_{abc}	V_{DGPS}	W_{abc}	W_{DGPS}			
ESA 1	2.4	20	2.5	4.6	2.3	1.1	11.6	6.9	27.9	16.7	0.60	0.34/2.1	Highest boulder, now resting at 10 m MLLW, vertical transport of 2.5 m, overturned
ESA 5	2.4	40	4	4.0	2.8	1.7	19.0	9.8	45.7	23.5	0.52	0.5/1.35	Vertical transport of 4 m, overturned, origin/fracture plain at 2 m MLLW
ESA 7	2.4	35	-	5.3	3. 0	2.9	46.1	28.5	110.7	68.6	0.62	0.73/0.85	Upper littoral, lateral transport by rolling/saltation, overturned
ESA 8	2.4	>40	>2.5	3.6	2.70	1.80	17.5	9.1	42.0	21.8	0.52	0.58/1.1	Living barnacles and boring valves (former intertidal), overturned, assumed vertical transport of at least 2.5 m
ESA 9	2.4	45	-	9.00	4.50	3.50	121.5	75.3*	291.6	180.8*	(0.62~~)~~*)[a]	0.55/1.4	Largest block, upper intertidal, lateral transport by sliding

Figure captions

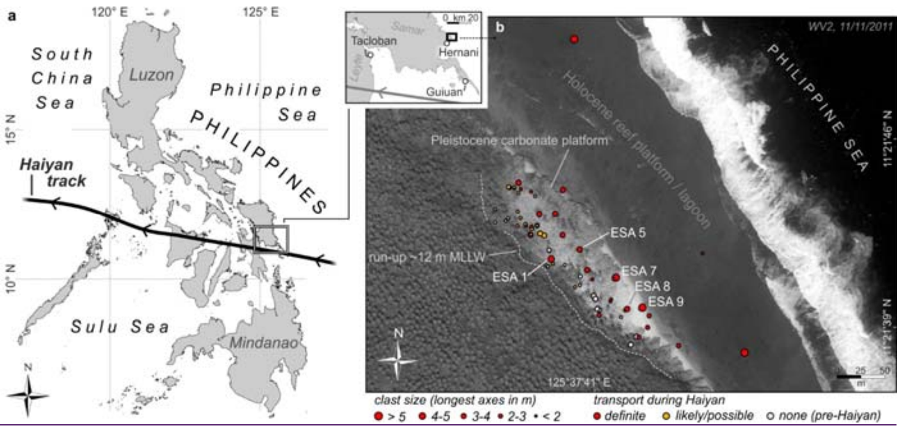

Figure 1: Study area and boulder field at site ESA. (a) Location of study area and Haiyan's track. (b) Setting of the boulder field at site ESA (59 clasts documented). The post-Haiyan image illustrates the extent of destroyed vegetation and deposited sand (light grey, on top of the Pleistocene carbonate platform) (WV2, 11/11/2013). Large clasts were moved on top of the Holocene reef as well as on top of the Pleistocene platform. A number of boulders (~30 clasts) were definitely transported, and dislocation of several further boulders is very likely. Further clasts must have been transported during an older palaeo-wave event.

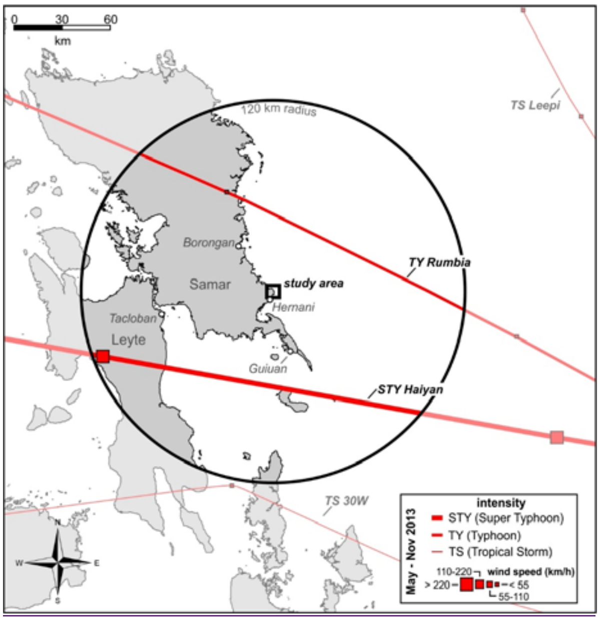

Figure 2: Previous typhoons and tropical storms. Location of study area, track of Supertyphoon Haiyan, and tracks of three further storm systems which occurred within an area of c. 250 km N, S, and E of ~~E Samar~~Eastern Samar between 4 May 2013 and 11 Nov 2013. (JTWC 2014). Tropical storm 30W (3 Nov–06 Nov 2013) and Typhoon Rumbia (27 Jun–02 Jul 2013) only reached moderate wind speeds of ≤65 km h^{-1} and atmospheric pressures of >995 hPa when passing the 120 km radius around the study area.

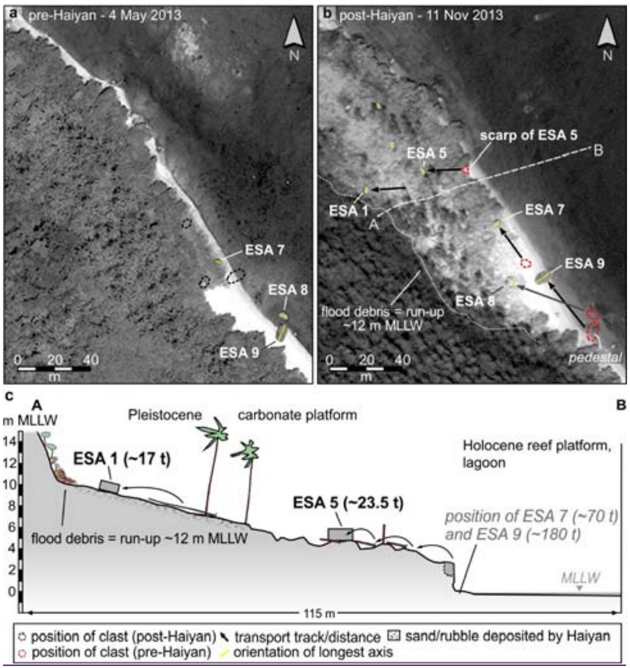

Figure 3: Large clasts transported by Haiyan at site ESA. (a,b) Pre- (WV1, 4/5/2013) and post-Haiyan images (WV2, 11/11/2013) ~~documenting~~ illustrating run-up extent, position of clasts ESA 1, 5, 7, 8 and 9, and trajectories. Transport direction of largest clasts ESA 7 and 9 is SE–NW, ~~coinciding with modeled flow vectors (Fig. 8) and, thus, with surge-accompanying water currents~~documenting a NW-directed surge. ESA 9 was moved by ~40 m. (c) Transect A–B. Flood debris at 12 m MLLW indicate maximum run-up. ESA 5: quarried from cliff edge.

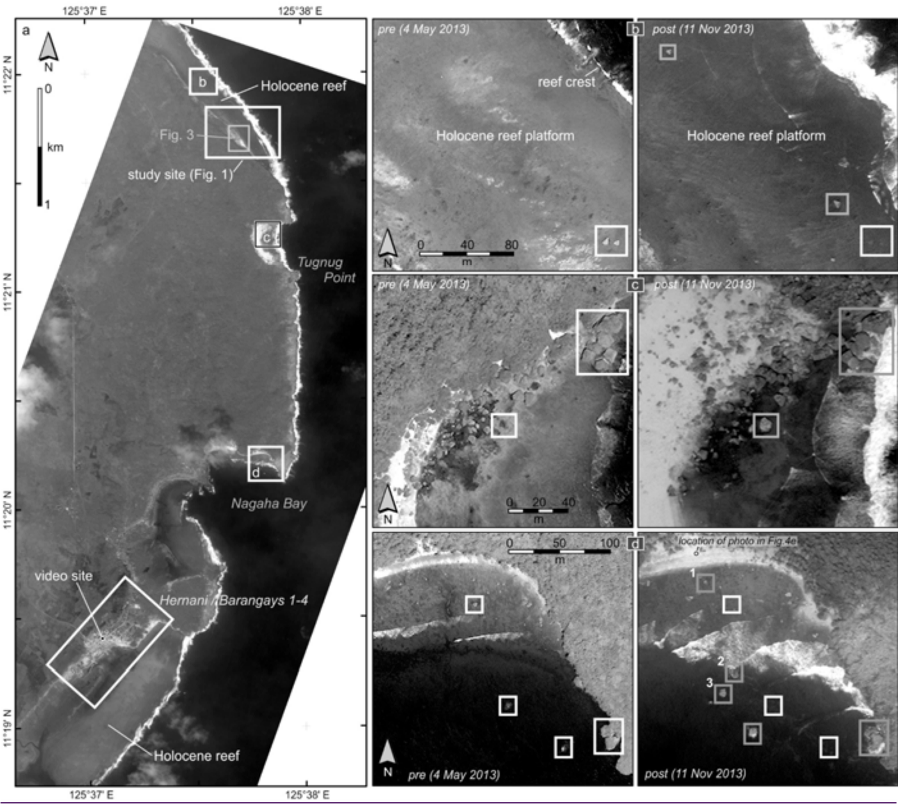

Figure 4: Further evidence of block and boulder transport during Haiyan. (a) Location of study site ESA (see also Figs. 1 and 3), the City of Hernani including the location of the eyewitness footage (Gensis; 2013), and further sites (b–d) with evidence for Haiyan-induced block and boulder transport. (b) Two triangle-shaped blocks (with axis >4 and >5 m) were shifted on top of the Holocene reef platform, some 500 m north of site ESA; a distance of >240 m is inferred for the smaller one. (c,d) South of ESA numerous large clasts of pre-existing boulder fields changed position. Note dislocation (post-Haiyan imbrication) of large blocks (longest axis >10 m) directly west of the headland and of intertidal clasts to the west; clasts marked by 1–3 are shown in Fig. 5e (d). White boxes mark pre-Haiyan positions, grey boxes post-Haiyan positions of clasts, or areas showing apparent movements of large clasts.

Figure 5: Photos of largest Haiyan-transported clasts at ESA. (a) Photo of ESA 9, the largest clast found at site ESA. (b) A ~5 cm high pedestal (foreground) was found at the pre-Haiyan position of ESA 9 (background). (c) Photo of ESA 7 looking from the SW towards the lagoon. (d) Boulder ESA 1, situated at ~10 m MLLW, directly below the run-up limit. (e) Panorama photo of Nagaha Bay (March 2015), view is to the SSE. Clasts 1–3 were dislocated by Haiyan, as documented by post-Haiyan satellite images (cf. Fig. 4d).

Figure 6: Indicators of boulder movement during typhoon Haiyan. (a) Origin of boulder ESA 5, quarried from the cliff at ~2 m MLLW and transported upwards and landwards for 4 m and 40 m, respectively. Snapped trees and impact marks on the carbonate platform can be traced on its trajectory. (b) Boulder at 6 m MLLW lying on top of freshly toppled palm trees. (c) Piece of wood jammed under boulder ESA 7. (d) Downward-facing and decaying grass patches at the former surface and new bottom side of ESA 7. (e) Percussion marks on the Pleistocene carbonate platform, tracing the transport track of ESA 5. Scale is 2 m. (f) Still living barnacle attached to boulder ESA 8, situated at 2.5 m MLLW, i.e. clearly above highest tide levels. (g) Roots and soil staining on the exposed former bottom side of several boulders (here boulder ESA 1) provide evidence of overturning during Haiyan.

Formatiert: Block, Abstand Vor: 6 Pt., Zeilenabstand: 1,5 Zeilen

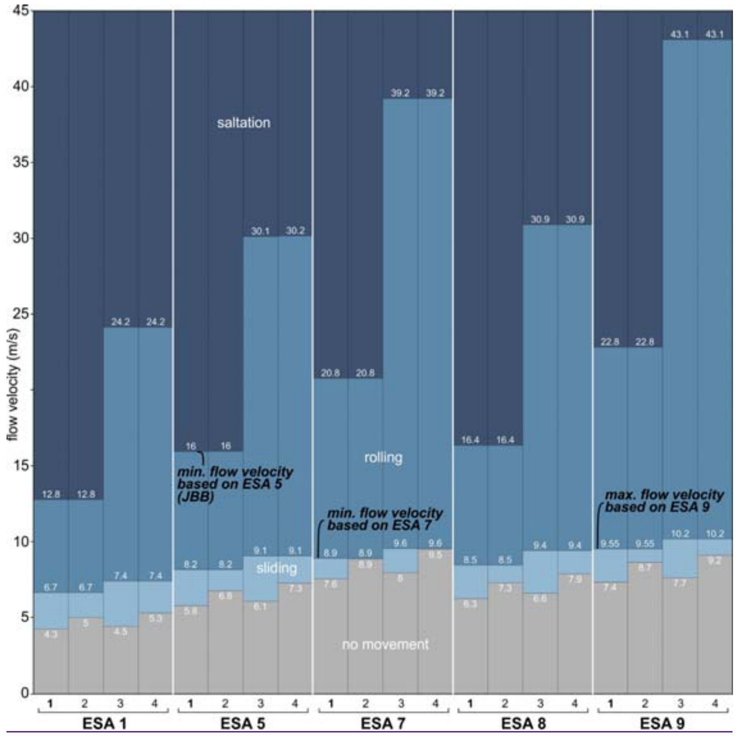

Figure 7: Flow velocities calculated for transport of largest clasts at site ESA. For each clast, flow velocities were calculated with different coefficients taken from literature (cases 1–4 on x-axis): 1 – C_l = 0.178, μ = 0.7; 2 – C_l = 0.178, μ = 1.02; 3 – C_l = 0.05, μ = 0.7; 4 – C_l = 0.05, μ = 1.02 (Nott, 2003; Noormets et al., 2004; Benner et al., 2010; Nandasena et al., 2011). For case 1, ~~For ESA 7,~~ minimum flow velocities of ~~6~~8.~~23~~9 m s-1 were calculated for ESA 7 using Eq. (2) to initiate rolling movement as observed in the field. ~~, which is similar to 6.33 m s-1 required to shift ESA 9.~~ Since no signs for overturning were documented for ESA 9, flow velocities are assumed to have remained below ~~8~~9.~~3~~55 m s-1 based on using Eq. (1). However, based on the Eq. (3) of Nandasena et al. (2011), quarrying of ESA 5 required flow velocities of >~~15~~16 m s-1. In comparison to case 1, flow velocities calculated for cases 2 – 4 differ in the order of 1.0 – 1.9 m s-1 (for the initiation of sliding) and 0.7-0.9 m s-1 (for the initiation of rolling). Remarkably higher flow velocities for the initiation of saltation are calculated with C_l = 0.05 (cases 3 and 4).

Formatiert: Nicht Hervorheben

Formatiert: Nicht Hervorheben

Formatiert: Schriftart: Kursiv

Formatiert: Nicht Hochgestellt/ Tiefgestellt

Formatiert: Schriftart: Kursiv

Formatiert: Nicht Hervorheben

Formatiert: Nicht Hervorheben

Formatiert: Nicht Hervorheben

Formatiert: Nicht Hervorheben

Formatiert: Nicht Hervorheben

Formatiert: Nicht Hervorheben

Formatiert: Nicht Hervorheben

Formatiert: Nicht Hervorheben

Formatiert: Nicht Hervorheben

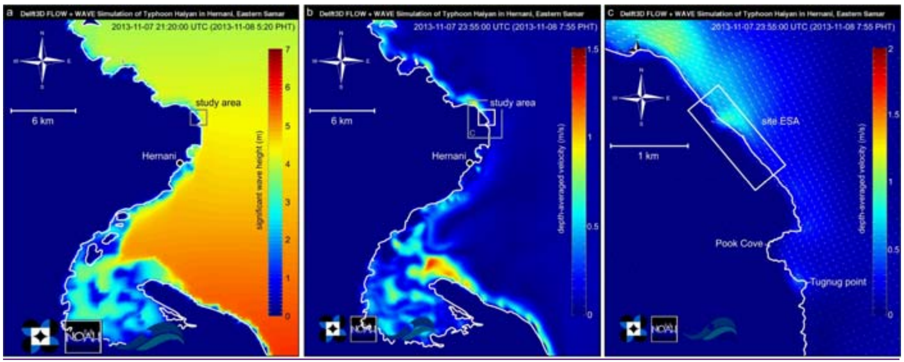

Figure 8: Results from the (phase-averaged) wave and storm surge model using Delft3D and Delft Dashboard software. (a) Maximum significant wave heights in ~~E Samar~~Eastern Samar. Based on our model, ~~In the study area,~~ max. significant waves heights reached c. 4-5 m at ~5~~.~~:20 a~~.~~m~~.~~ PHT~~.~~ in the study area. However, wave heights seem to be underestimated when compared to previously published low resolution models (Bricker et al., 2014; Fig. 3). (b,c) Even in the coupled hydrodynamic and wave model, combining pressure- and wind-driven surge as well as wave setup, the max. depth-averaged flow velocities calculated for ~~E Samar~~Eastern Samar (b) and the study area (c) remain below 1.5 m s^{-1}. Highest velocities at ESA are approached at ~8~~.~~:00 a~~.~~m~~.~~ PHT. PHT – Philippines Time; UTC - Coordinated Universal Time.

Formatiert: Englisch (USA)

Formatiert: Hochgestellt

Seite 13: [1] Formatiert **Matthias May** **14.11.2015 20:25:00**

Nicht Hervorheben

Seite 13: [1] Formatiert **Matthias May** **14.11.2015 20:25:00**

Nicht Hervorheben

Seite 13: [1] Formatiert **Matthias May** **14.11.2015 20:25:00**

Nicht Hervorheben

Seite 13: [1] Formatiert **Matthias May** **14.11.2015 20:25:00**

Nicht Hervorheben

Seite 13: [1] Formatiert **Matthias May** **14.11.2015 20:25:00**

Nicht Hervorheben

Seite 13: [1] Formatiert **Matthias May** **14.11.2015 20:25:00**

Nicht Hervorheben

Seite 13: [1] Formatiert **Matthias May** **14.11.2015 20:25:00**

Nicht Hervorheben

Seite 13: [1] Formatiert **Matthias May** **14.11.2015 20:25:00**

Nicht Hervorheben

Seite 13: [1] Formatiert **Matthias May** **14.11.2015 20:25:00**

Nicht Hervorheben

Seite 13: [1] Formatiert **Matthias May** **14.11.2015 20:25:00**

Nicht Hervorheben

Seite 13: [1] Formatiert **Matthias May** **14.11.2015 20:25:00**

Nicht Hervorheben

Seite 13: [1] Formatiert **Matthias May** **14.11.2015 20:25:00**

Nicht Hervorheben

Seite 13: [1] Formatiert **Matthias May** **14.11.2015 20:25:00**

Nicht Hervorheben

Seite 13: [1] Formatiert **Matthias May** **14.11.2015 20:25:00**

Nicht Hervorheben

Seite 13: [1] Formatiert	Matthias May	14.11.2015 20:25:00

Nicht Hervorheben

Seite 13: [1] Formatiert	Matthias May	14.11.2015 20:25:00

Nicht Hervorheben

Seite 13: [1] Formatiert	Matthias May	14.11.2015 20:25:00

Nicht Hervorheben

Seite 13: [1] Formatiert	Matthias May	14.11.2015 20:25:00

Nicht Hervorheben

Seite 13: [1] Formatiert	Matthias May	14.11.2015 20:25:00

Nicht Hervorheben

Seite 13: [1] Formatiert	Matthias May	14.11.2015 20:25:00

Nicht Hervorheben

Seite 13: [1] Formatiert	Matthias May	14.11.2015 20:25:00

Nicht Hervorheben

Seite 13: [1] Formatiert	Matthias May	14.11.2015 20:25:00

Nicht Hervorheben

Seite 13: [1] Formatiert	Matthias May	14.11.2015 20:25:00

Nicht Hervorheben

Seite 13: [2] Formatiert	May	03.11.2015 16:34:00

Nicht Hervorheben

Seite 13: [2] Formatiert	May	03.11.2015 16:34:00

Nicht Hervorheben

Seite 13: [2] Formatiert	May	03.11.2015 16:34:00

Nicht Hervorheben

Seite 13: [2] Formatiert	May	03.11.2015 16:34:00

Nicht Hervorheben

Seite 13: [2] Formatiert	May	03.11.2015 16:34:00

Nicht Hervorheben

Seite 13: [2] Formatiert **May** **03.11.2015 16:34:00**

Nicht Hervorheben

Seite 13: [3] Formatiert **May** **03.11.2015 16:34:00**

Schriftart: (Standard) Times New Roman, 12 Pt., Schriftfarbe: Schwarz

Seite 13: [3] Formatiert **May** **03.11.2015 16:34:00**

Schriftart: (Standard) Times New Roman, 12 Pt., Schriftfarbe: Schwarz

Seite 13: [3] Formatiert **May** **03.11.2015 16:34:00**

Schriftart: (Standard) Times New Roman, 12 Pt., Schriftfarbe: Schwarz

Seite 13: [3] Formatiert **May** **03.11.2015 16:34:00**

Schriftart: (Standard) Times New Roman, 12 Pt., Schriftfarbe: Schwarz

Seite 13: [3] Formatiert **May** **03.11.2015 16:34:00**

Schriftart: (Standard) Times New Roman, 12 Pt., Schriftfarbe: Schwarz

Seite 13: [3] Formatiert **May** **03.11.2015 16:34:00**

Schriftart: (Standard) Times New Roman, 12 Pt., Schriftfarbe: Schwarz

Seite 13: [4] Formatiert **May** **30.10.2015 15:46:00**

Schriftart: (Standard) Times New Roman, 12 Pt., Schriftfarbe: Schwarz

Seite 13: [4] Formatiert **May** **30.10.2015 15:46:00**

Schriftart: (Standard) Times New Roman, 12 Pt., Schriftfarbe: Schwarz

Seite 13: [4] Formatiert **May** **30.10.2015 15:46:00**

Schriftart: (Standard) Times New Roman, 12 Pt., Schriftfarbe: Schwarz

Seite 13: [4] Formatiert **May** **30.10.2015 15:46:00**

Schriftart: (Standard) Times New Roman, 12 Pt., Schriftfarbe: Schwarz

Seite 13: [5] Formatiert **May** **16.11.2015 15:17:00**

Schriftart: (Standard) Times New Roman, 12 Pt., Schriftfarbe: Schwarz

Seite 13: [5] Formatiert **May** **16.11.2015 15:17:00**

Schriftart: (Standard) Times New Roman, 12 Pt., Schriftfarbe: Schwarz

Seite 13: [5] Formatiert **May** **16.11.2015 15:17:00**

Schriftart: (Standard) Times New Roman, 12 Pt., Schriftfarbe: Schwarz

Seite 13: [5] Formatiert **May** **16.11.2015 15:17:00**

Schriftart: (Standard) Times New Roman, 12 Pt., Schriftfarbe: Schwarz

Seite 13: [5] Formatiert **May** **16.11.2015 15:17:00**

Schriftart: (Standard) Times New Roman, 12 Pt., Schriftfarbe: Schwarz

Seite 13: [5] Formatiert **May** **16.11.2015 15:17:00**

Schriftart: (Standard) Times New Roman, 12 Pt., Schriftfarbe: Schwarz

Seite 13: [5] Formatiert **May** **16.11.2015 15:17:00**

Schriftart: (Standard) Times New Roman, 12 Pt., Schriftfarbe: Schwarz

Seite 13: [5] Formatiert **May** **16.11.2015 15:17:00**

Schriftart: (Standard) Times New Roman, 12 Pt., Schriftfarbe: Schwarz

Seite 13: [5] Formatiert **May** **16.11.2015 15:17:00**

Schriftart: (Standard) Times New Roman, 12 Pt., Schriftfarbe: Schwarz

Seite 13: [5] Formatiert **May** **16.11.2015 15:17:00**

Schriftart: (Standard) Times New Roman, 12 Pt., Schriftfarbe: Schwarz

Seite 13: [5] Formatiert **May** **16.11.2015 15:17:00**

Schriftart: (Standard) Times New Roman, 12 Pt., Schriftfarbe: Schwarz

Seite 13: [5] Formatiert **May** **16.11.2015 15:17:00**

Schriftart: (Standard) Times New Roman, 12 Pt., Schriftfarbe: Schwarz

Seite 13: [5] Formatiert **May** **16.11.2015 15:17:00**

Schriftart: (Standard) Times New Roman, 12 Pt., Schriftfarbe: Schwarz

Seite 13: [5] Formatiert **May** **16.11.2015 15:17:00**

Schriftart: (Standard) Times New Roman, 12 Pt., Schriftfarbe: Schwarz

Seite 13: [5] Formatiert **May** **16.11.2015 15:17:00**

Schriftart: (Standard) Times New Roman, 12 Pt., Schriftfarbe: Schwarz

Seite 13: [5] Formatiert **May** **16.11.2015 15:17:00**

Schriftart: (Standard) Times New Roman, 12 Pt., Schriftfarbe: Schwarz

Seite 13: [5] Formatiert **May** **16.11.2015 15:17:00**

Schriftart: (Standard) Times New Roman, 12 Pt., Schriftfarbe: Schwarz

Seite 13: [5] Formatiert	May	16.11.2015 15:17:00

Schriftart: (Standard) Times New Roman, 12 Pt., Schriftfarbe: Schwarz

Seite 13: [5] Formatiert	May	16.11.2015 15:17:00

Schriftart: (Standard) Times New Roman, 12 Pt., Schriftfarbe: Schwarz

Seite 13: [5] Formatiert	May	16.11.2015 15:17:00

Schriftart: (Standard) Times New Roman, 12 Pt., Schriftfarbe: Schwarz

Seite 13: [5] Formatiert	May	16.11.2015 15:17:00

Schriftart: (Standard) Times New Roman, 12 Pt., Schriftfarbe: Schwarz

Seite 13: [5] Formatiert	May	16.11.2015 15:17:00

Schriftart: (Standard) Times New Roman, 12 Pt., Schriftfarbe: Schwarz

Seite 13: [5] Formatiert	May	16.11.2015 15:17:00

Schriftart: (Standard) Times New Roman, 12 Pt., Schriftfarbe: Schwarz

Seite 13: [5] Formatiert	May	16.11.2015 15:17:00

Schriftart: (Standard) Times New Roman, 12 Pt., Schriftfarbe: Schwarz

Seite 13: [5] Formatiert	May	16.11.2015 15:17:00

Schriftart: (Standard) Times New Roman, 12 Pt., Schriftfarbe: Schwarz

Seite 13: [5] Formatiert	May	16.11.2015 15:17:00

Schriftart: (Standard) Times New Roman, 12 Pt., Schriftfarbe: Schwarz

Seite 13: [5] Formatiert	May	16.11.2015 15:17:00

Schriftart: (Standard) Times New Roman, 12 Pt., Schriftfarbe: Schwarz

Seite 13: [5] Formatiert	May	16.11.2015 15:17:00

Schriftart: (Standard) Times New Roman, 12 Pt., Schriftfarbe: Schwarz

Seite 13: [5] Formatiert	May	16.11.2015 15:17:00

Schriftart: (Standard) Times New Roman, 12 Pt., Schriftfarbe: Schwarz

Seite 13: [5] Formatiert	May	16.11.2015 15:17:00

Schriftart: (Standard) Times New Roman, 12 Pt., Schriftfarbe: Schwarz

Seite 13: [5] Formatiert	May	16.11.2015 15:17:00

Schriftart: (Standard) Times New Roman, 12 Pt., Schriftfarbe: Schwarz

Seite 13: [5] Formatiert **May** **16.11.2015 15:17:00**

Schriftart: (Standard) Times New Roman, 12 Pt., Schriftfarbe: Schwarz

Seite 13: [5] Formatiert **May** **16.11.2015 15:17:00**

Schriftart: (Standard) Times New Roman, 12 Pt., Schriftfarbe: Schwarz

Seite 13: [5] Formatiert **May** **16.11.2015 15:17:00**

Schriftart: (Standard) Times New Roman, 12 Pt., Schriftfarbe: Schwarz

Seite 13: [5] Formatiert **May** **16.11.2015 15:17:00**

Schriftart: (Standard) Times New Roman, 12 Pt., Schriftfarbe: Schwarz

Seite 13: [5] Formatiert **May** **16.11.2015 15:17:00**

Schriftart: (Standard) Times New Roman, 12 Pt., Schriftfarbe: Schwarz

Seite 13: [5] Formatiert **May** **16.11.2015 15:17:00**

Schriftart: (Standard) Times New Roman, 12 Pt., Schriftfarbe: Schwarz

Seite 13: [5] Formatiert **May** **16.11.2015 15:17:00**

Schriftart: (Standard) Times New Roman, 12 Pt., Schriftfarbe: Schwarz

Seite 13: [5] Formatiert **May** **16.11.2015 15:17:00**

Schriftart: (Standard) Times New Roman, 12 Pt., Schriftfarbe: Schwarz

Seite 14: [6] Formatiert **May** **16.11.2015 15:17:00**

Englisch (Großbritannien)

Seite 14: [6] Formatiert **May** **16.11.2015 15:17:00**

Englisch (Großbritannien)

Seite 14: [6] Formatiert **May** **16.11.2015 15:17:00**

Englisch (Großbritannien)

Seite 14: [6] Formatiert **May** **16.11.2015 15:17:00**

Englisch (Großbritannien)

Seite 14: [7] Formatiert **May** **16.11.2015 15:17:00**

Nicht Hervorheben

Seite 14: [7] Formatiert **May** **16.11.2015 15:17:00**

Nicht Hervorheben

Seite 14: [7] Formatiert	May	16.11.2015 15:17:00

Nicht Hervorheben

Seite 14: [7] Formatiert	May	16.11.2015 15:17:00

Nicht Hervorheben

Seite 14: [7] Formatiert	May	16.11.2015 15:17:00

Nicht Hervorheben

Seite 14: [7] Formatiert	May	16.11.2015 15:17:00

Nicht Hervorheben

Seite 14: [7] Formatiert	May	16.11.2015 15:17:00

Nicht Hervorheben

Seite 14: [7] Formatiert	May	16.11.2015 15:17:00

Nicht Hervorheben

Seite 14: [7] Formatiert	May	16.11.2015 15:17:00

Nicht Hervorheben

Seite 14: [7] Formatiert	May	16.11.2015 15:17:00

Nicht Hervorheben

Seite 14: [7] Formatiert	May	16.11.2015 15:17:00

Nicht Hervorheben

Seite 14: [7] Formatiert	May	16.11.2015 15:17:00

Nicht Hervorheben

Seite 14: [7] Formatiert	May	16.11.2015 15:17:00

Nicht Hervorheben

Seite 14: [7] Formatiert	May	16.11.2015 15:17:00

Nicht Hervorheben

Seite 14: [7] Formatiert	May	16.11.2015 15:17:00

Nicht Hervorheben

Seite 14: [7] Formatiert	May	16.11.2015 15:17:00

Nicht Hervorheben

Seite 14: [7] Formatiert **May** **16.11.2015 15:17:00**

Nicht Hervorheben

Seite 14: [7] Formatiert **May** **16.11.2015 15:17:00**

Nicht Hervorheben

Seite 14: [7] Formatiert **May** **16.11.2015 15:17:00**

Nicht Hervorheben

Seite 14: [7] Formatiert **May** **16.11.2015 15:17:00**

Nicht Hervorheben

Seite 14: [7] Formatiert **May** **16.11.2015 15:17:00**

Nicht Hervorheben

Seite 14: [7] Formatiert **May** **16.11.2015 15:17:00**

Nicht Hervorheben

Seite 14: [7] Formatiert **May** **16.11.2015 15:17:00**

Nicht Hervorheben

Seite 14: [7] Formatiert **May** **16.11.2015 15:17:00**

Nicht Hervorheben

Seite 14: [7] Formatiert **May** **16.11.2015 15:17:00**

Nicht Hervorheben

Seite 14: [7] Formatiert **May** **16.11.2015 15:17:00**

Nicht Hervorheben

Seite 14: [7] Formatiert **May** **16.11.2015 15:17:00**

Nicht Hervorheben

Seite 14: [7] Formatiert **May** **16.11.2015 15:17:00**

Nicht Hervorheben

Seite 14: [8] Formatiert **May** **16.11.2015 15:17:00**

Nicht Hervorheben

Seite 14: [8] Formatiert **May** **16.11.2015 15:17:00**

Nicht Hervorheben

Seite 14: [8] Formatiert	May	16.11.2015 15:17:00

Nicht Hervorheben

Seite 14: [8] Formatiert	May	16.11.2015 15:17:00

Nicht Hervorheben

Seite 14: [8] Formatiert	May	16.11.2015 15:17:00

Nicht Hervorheben

Seite 14: [9] Formatiert	May	16.11.2015 15:17:00

Nicht Hervorheben

Seite 14: [9] Formatiert	May	16.11.2015 15:17:00

Nicht Hervorheben

Seite 14: [10] Formatiert	Matthias May	13.11.2015 00:26:00

Nicht Hervorheben

Seite 14: [10] Formatiert	Matthias May	13.11.2015 00:26:00

Nicht Hervorheben

Seite 14: [10] Formatiert	Matthias May	13.11.2015 00:26:00

Nicht Hervorheben

Seite 14: [10] Formatiert	Matthias May	13.11.2015 00:26:00

Nicht Hervorheben

Seite 14: [10] Formatiert	Matthias May	13.11.2015 00:26:00

Nicht Hervorheben

Seite 14: [11] Formatiert	A	16.11.2015 16:26:00

Hochgestellt

Seite 14: [11] Formatiert	A	16.11.2015 16:26:00

Hochgestellt

Seite 14: [12] Formatiert	May	30.10.2015 15:43:00

Nicht Hervorheben

Seite 14: [12] Formatiert	May	30.10.2015 15:43:00

Nicht Hervorheben

Seite 14: [13] Formatiert	May	30.10.2015 15:46:00

Nicht Hervorheben

Seite 14: [13] Formatiert	May	30.10.2015 15:46:00

Nicht Hervorheben